PHILOSOPHICAL TRANSACTIONS OF THE ROYAL SOCIETY A MATHEMATICAL, PHYSICAL & ENGINEERING SCIENCES

The X-Ray Corona from Skylab

G. S. Vaiana

Phil. Trans. R. Soc. Lond. A 1976 **281**, 365-374
doi: 10.1098/rsta.1976.0034

Phil. Trans. R. Soc. Lond. A. **281**, 365–374 (1976) [365]
Printed in Great Britain

The X-ray corona from Skylab

By G. S. Vaiana
Center for Astrophysics, Harvard College Observatory, Cambridge, Massachusetts, U.S.A.

[Plates 16–21]

An overview of the images obtained with the A.S. & E. X-ray telescope on Skylab shows the low corona to be highly structured. The plasma is distributed in closed loops shaped by the magnetic field with sizes ranging from the smallest resolvable structures of a few thousand kilometres to loops that reach halfway across the solar disk. Relatively high-temperature and dense plasma loops overlay active regions; large-scale interconnections link active regions to their surrounding fields and in some cases to other active regions. The large-scale loops, which cover most of the Sun outside of active regions, appear to be related to old active regions whose magnetic fields have spread out over the course of several solar rotations. Often at the poles and occasionally on the disk, large regions display radial field configurations (coronal holes) from which the plasma preferentially escapes into high-velocity solar wind streams.

A comprehensive view of the structure and evolution of the X-ray corona is given in terms of the physical conditions existing in the various coronal loops, and the importance of active regions is emphasized by examining their structure and time development over a wide range of scales.

1. Introduction

We review here some of the recent results obtained with the A.S. & E. X-ray telescope on Skylab and present an overall view of the low corona as seen in X-rays,† with emphasis on the role of active regions.

Our instrument was a result of many years of development at A.S. & E. and the analysis of the large quantity of data is done by a team of people both at A.S. & E. and at the Center for Astrophysics. The telescope (figure 1) is a grazing incidence instrument with spatial resolution of the order of 2″ (see Vaiana *et al.* 1974*b* for a more complete description) with optics that are a nested configuration of two mirrors in order to increase the collecting area. Six broadband filters define (together with the short wavelength cut-off of the mirror) portions of the spectral range of the instrument within the total observable wavelength range of 2–60 Å. The transmission of each as a function of wavelength is indicated in figure 2. Images were recorded on photographic film.

Five magazines were used during the Skylab mission, and a total of 32 000 exposures was obtained. The instrument was also used with an X-ray transmission grating to make objective grating spectroheliograms of small intense sources, such as flares; but for the purposes of this talk we will confine ourselves to the images obtained with the broadband filters.

The physical conditions in the solar corona are such that it emits primarily in the soft X-ray region of the spectrum. The dominant contributions are from resonance and high-ionization lines, and the corona is optically thin in soft X-rays, allowing us to see the emission integrated along the line of sight. The magnetic energy dominates over the thermal energy, allowing the

† Nomenclature and earlier rocket results are reviewed by Vaiana, Krieger & Timothy (1973*a*). Earlier reviews of the Skylab results have been presented at several meetings (see, for instance, Vaiana, Krieger, Timothy & Zombeck 1974*a*).

structure of the plasma to trace the field direction. Currents must also play a role, at least in supporting and stabilizing the plasma and in confining it in the narrow loops and tube structures that we see.

According to current thinking, the aspects most fundamental in establishing the dynamics of the solar atmosphere are: (1) the emergence of magnetic fields; (2) the dispersion of these fields by surface motions at chromospheric level; and (3) the onset of instabilities in the plasma.

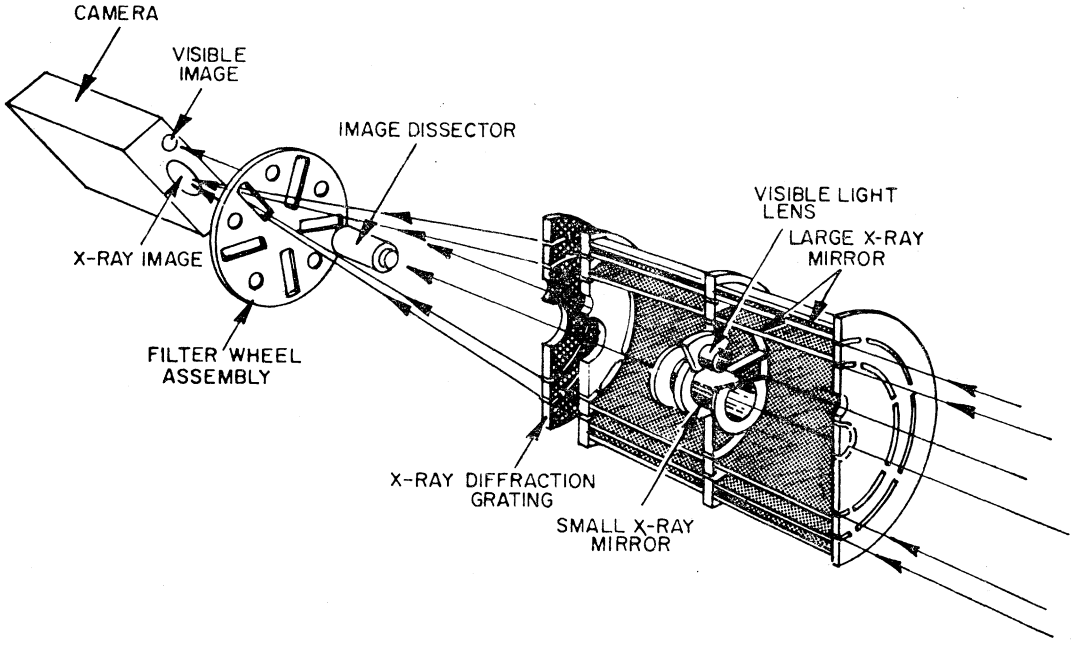

FIGURE 1. Schematic of the S-054 X-ray telescope.

Observations in the X-ray regions, by enabling the study of the physical condition of the coronal plasma, enable the form and distribution of the magnetic field in the corona to be observed as a function of time, from the emergence of a flux tube to the dissipation and/or dispersion in the background field and allow a study of these points to be made.

Furthermore, temperatures, densities, and characteristic time scales from the X-ray observations, together with measurements of the photospheric fields, can provide insight into the condition of force balance and energy balance and indicate which energy loss mechanisms may exist in the region.

Our instrument, therefore, was intended to provide a broad survey of the structures and the dynamics of X-ray emitting regions. We will discuss the general structure of the corona and the various features observed, with an eye towards the role played by active regions in contributing to this structuring. In more detail, we examine the various aspects of active regions, including the importance of loops for the entire range of size scales, from compact cores to large-scale loops, within active regions, and the dynamics involved in both short-term and long-term development of these regions. Also examined is the emergence of active regions. Structures in the corona, such as coronal holes and large-scale loops, are shown; and associations with magnetic fields in each of these contexts is studied, as well as the range of physical parameters involved.

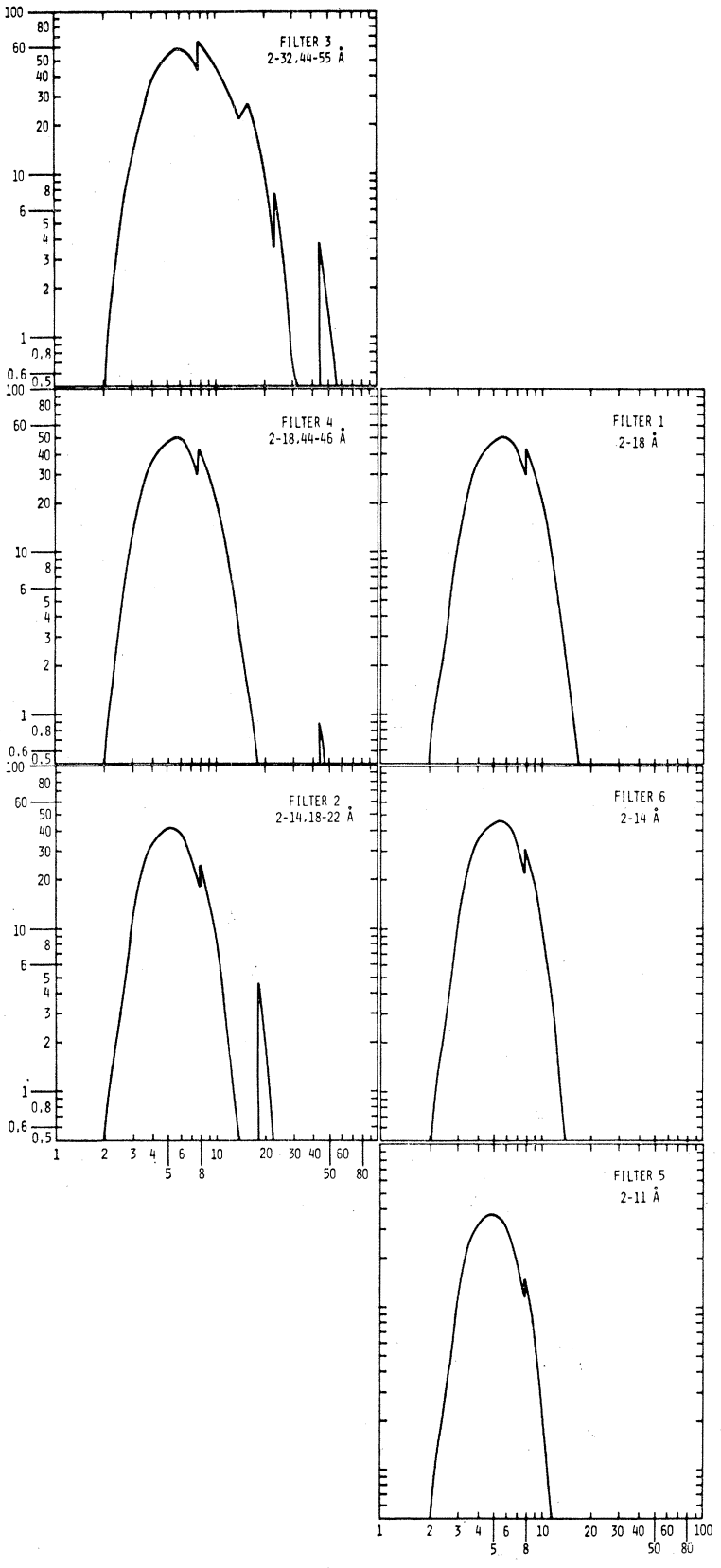

FIGURE 2. Transmission against wavelength for the six filters of the experiment

PHILOSOPHICAL TRANSACTIONS OF THE ROYAL SOCIETY A MATHEMATICAL, PHYSICAL & ENGINEERING SCIENCES

2. The data

A representative view of the X-ray corona is shown in figure 3, plate 16, through the broadest wavelength passband of the instrument (2–32 Å and 44–55 Å). In this soft filter the highly structured nature of the corona is immediately obvious. This is true not only in active regions but in the so-called 'quiet regions' as well. Clearly, one cannot speak of active regions as isolated structures. One can see the high-temperature plasma outlining the topology of the coronal magnetic fields. It is seen that the low corona, as shown by the X-ray emission, appears to be poorly described by any simple homogeneous, symmetrical model and that its structure exhibits an important relation to the development of active regions.

It is with exposures of this kind, in time sequences, that one studies the emergence, the development, and the decay of the fields as outlined by the plasma. The role of active regions in the development of the entire corona is seen to be a central one. In figure 3 the bright overexposed features are the high-temperature coronal structures of active regions. We discuss their structure in more detail later in this presentation. Larger-scale loops are also shown interconnecting active regions to their surrounding fields and sometimes to other active region fields.

The types of features represented in figure 3 have been studied by various investigators in our team and the results presented elsewhere. Tables 1 and 2 display some of the typical parameters calculated from the data. In reality a range of values occurs, but for the purposes of a general discussion, these values are representative. Temperatures, emission measures, column lengths of the radiating plasma, thermal energy densities, magnetic fields, and radiative lifetimes are presented in table 1. Table 2 gives the corresponding projected areas, total X-ray luminosities, X-ray fluxes at the Sun, total thermal energy contents, and masses for each feature.

Table 1

	(1) T_6/K	(2) $\int N_e^2 \mathrm{d}l/\mathrm{cm}^{-5}$	(3) $\int \mathrm{d}l/\mathrm{cm}$	(4) $\bar{N}_e/\mathrm{cm}^{-3}$	(5) $\frac{3NKT}{10^{-7}\,\mathrm{J\,cm}^{-3}}$	(6) $\frac{B_{eq}}{10^{-4}T}$	(7) t_{rad}
coronal hole	1.3†	3×10^{26}	6×10^{9}‡	2.2×10^{8}	0.1	2	1×10^{5}
large-scale structures	1.6	5×10^{27}	8×10^{9}§	8×10^{8}	0.5	4	4×10^{4}
bright point	1.6	1×10^{28}	7×10^{8}	3.8×10^{9}	2.5	9	9×10^{3}
active region	2.5	2×10^{29}	7×10^{9}	7×10^{9}	7	13	7×10^{3}
C-flare	10	2×10^{31}	2×10^{9}	1×10^{11}	400	100	2×10^{3}

† The value for the temperature of a coronal hole was not obtained directly, since no emission is seen in the harder filters, but is an estimate based on the emission observed in the softest filter only.
‡ The length parameter for a coronal hole is taken to be the density scale height.
§ The density scale height is used for the length parameter for the large-scale structure.

Table 2

	(1) A/cm^2	(2) $L/(10^{-7}\,\mathrm{J\,s}^{-1})$	(3) $\mathrm{d}L/\mathrm{d}A$	(4) $E_T/(10^{-7}\,\mathrm{J})$	(5) M/g
coronal hole	5×10^{21}†	3×10^{25}	6×10^{3}	3×10^{39}	1×10^{15}
large-scale structures	5×10^{22}‡	5×10^{27}	1×10^{5}	2×10^{32}	5×10^{17}
bright point	5×10^{17}	1×10^{23}	2×10^{5}	9×10^{26}	3×10^{12}
active region	2×10^{19}	8×10^{25}	4×10^{6}	6×10^{29}	1×10^{15}
C-flare	5×10^{18}	2×10^{27}	—	3×10^{30}	1.6×10^{15}

† The area assumed for a coronal hole is taken to be 10 % of the total solar surface area.
‡ The area used in these calculations assumes the entire solar surface is covered by large-scale structures.

PHILOSOPHICAL TRANSACTIONS OF THE ROYAL SOCIETY A MATHEMATICAL, PHYSICAL & ENGINEERING SCIENCES

PHILOSOPHICAL TRANSACTIONS OF THE ROYAL SOCIETY A MATHEMATICAL, PHYSICAL & ENGINEERING SCIENCES

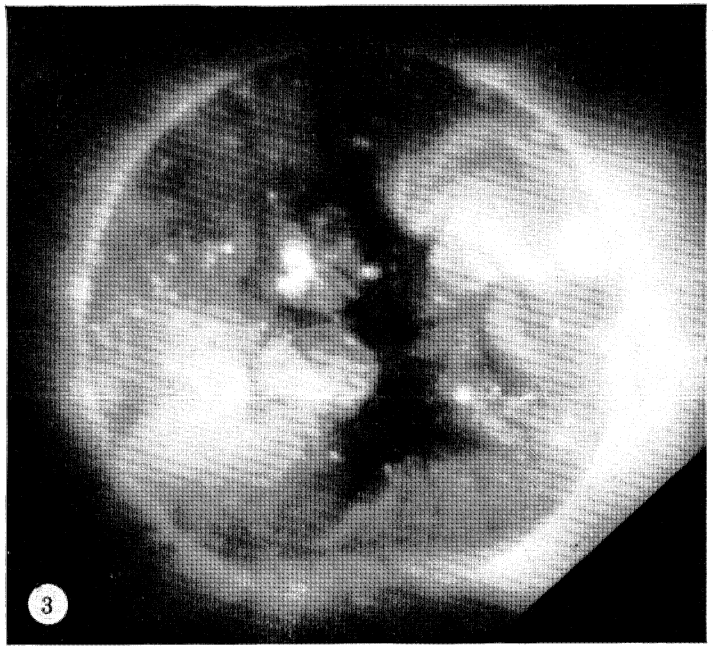

FIGURE 3. A full disk view of the X-ray corona on 1 June 1973.

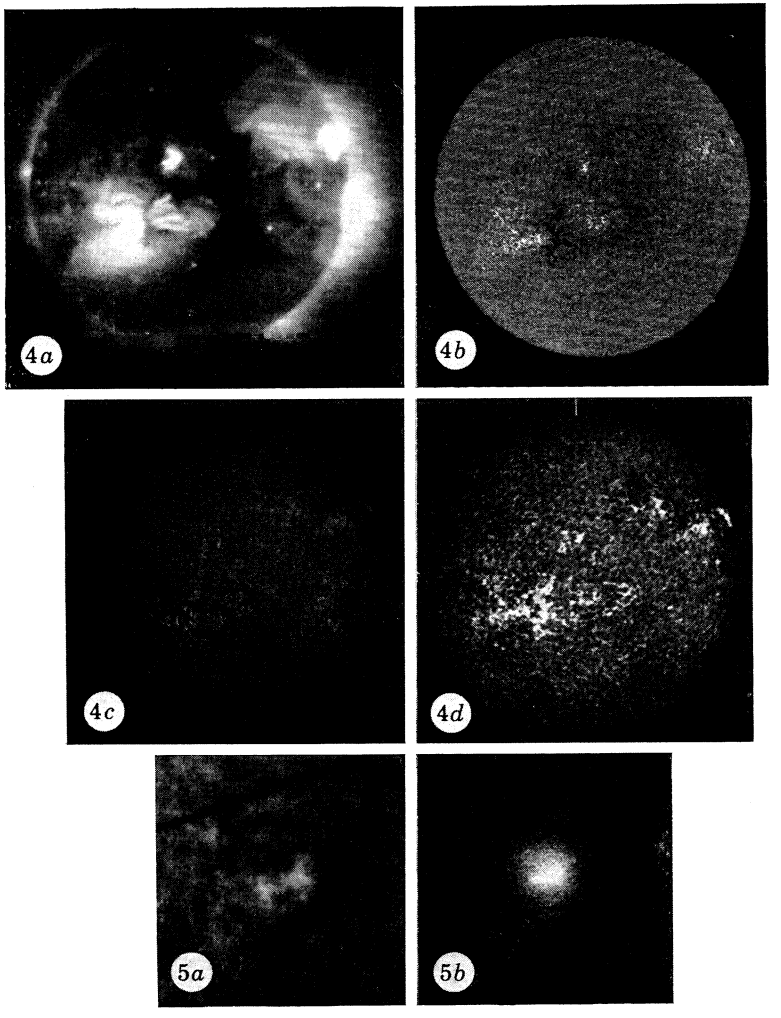

FIGURE 4. Comparison of (*a*) the X-ray corona showing the 1 June 1973 coronal hole with (*b*) the corresponding Kitt Peak magnetogram (courtesy of J. Harvey & W. Livingston), (*c*) an Hα image, and (*d*) a Ca K image for the same date.

FIGURE 5. (*a*) Hα and (*b*) X-ray images of a very simple active region (22:07:00 U.T. and 21:40:18 U.T. of 1 September 1973). Note the indication of a loop structure in the X-ray core.

(*Facing p.* 368)

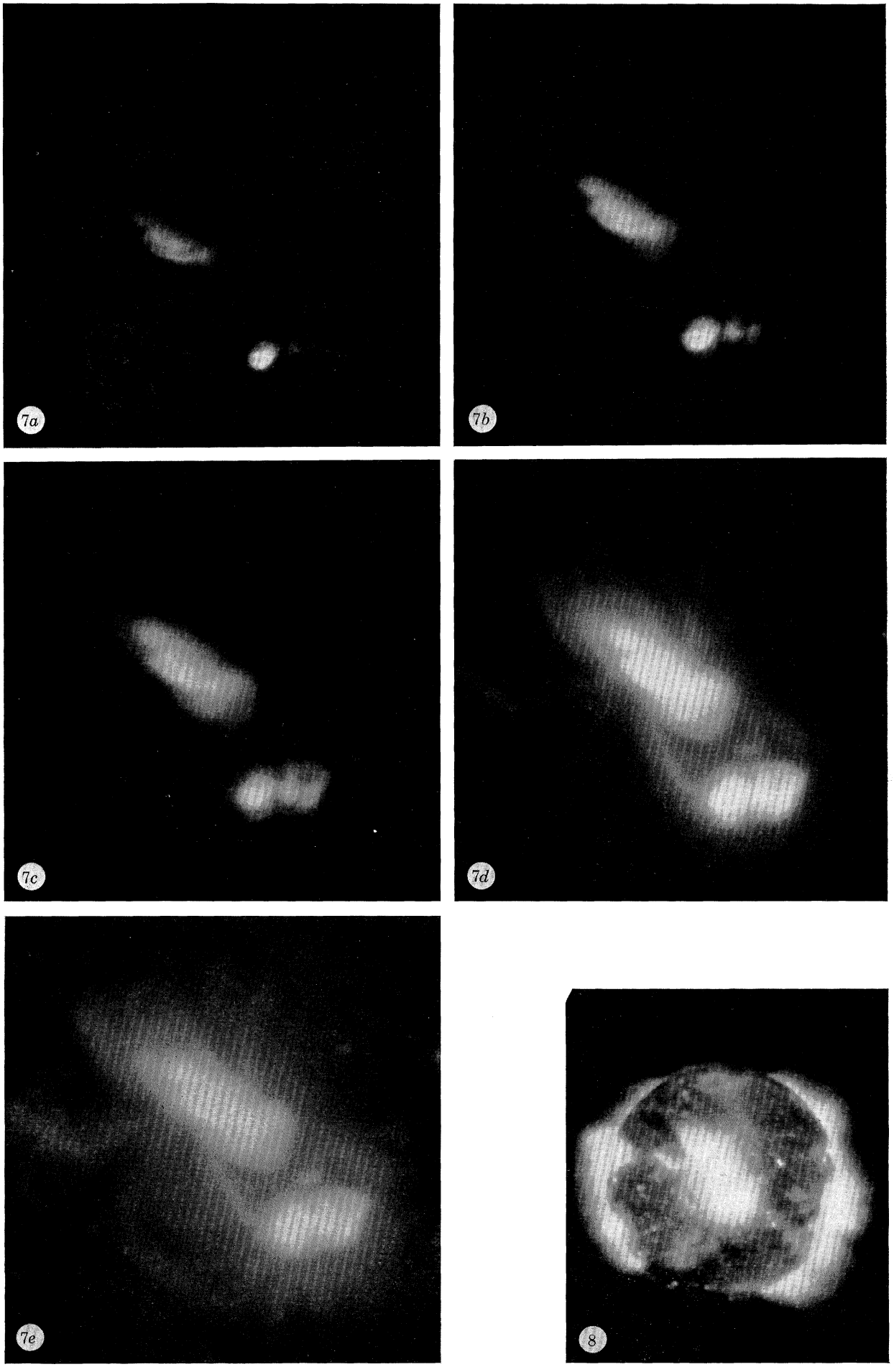

FIGURES 7 AND 8. For description see opposite.

PHILOSOPHICAL TRANSACTIONS OF THE ROYAL SOCIETY A MATHEMATICAL, PHYSICAL & ENGINEERING SCIENCES

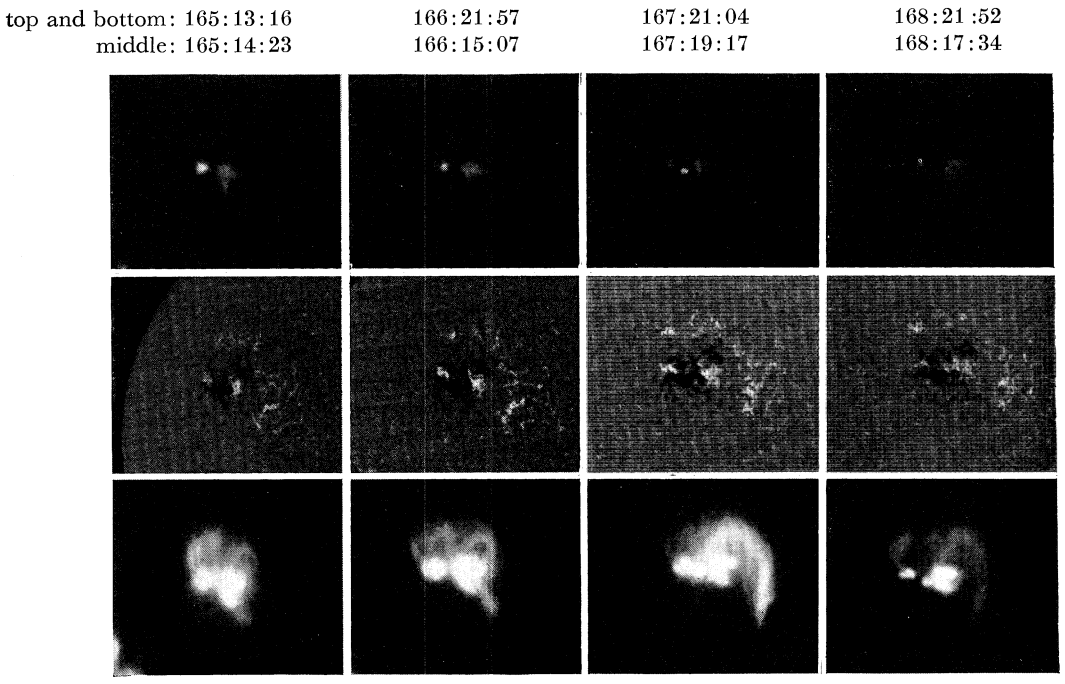

FIGURE 6. A three-day development of an active region from 14 June to 17 June 1973. Both the X-ray images (hard filter, two exposures, top and bottom rows) and the Kitt Peak magnetograms (middle row) are shown. The field is approximately 4×10^5 km by 5×10^5 km for each image.

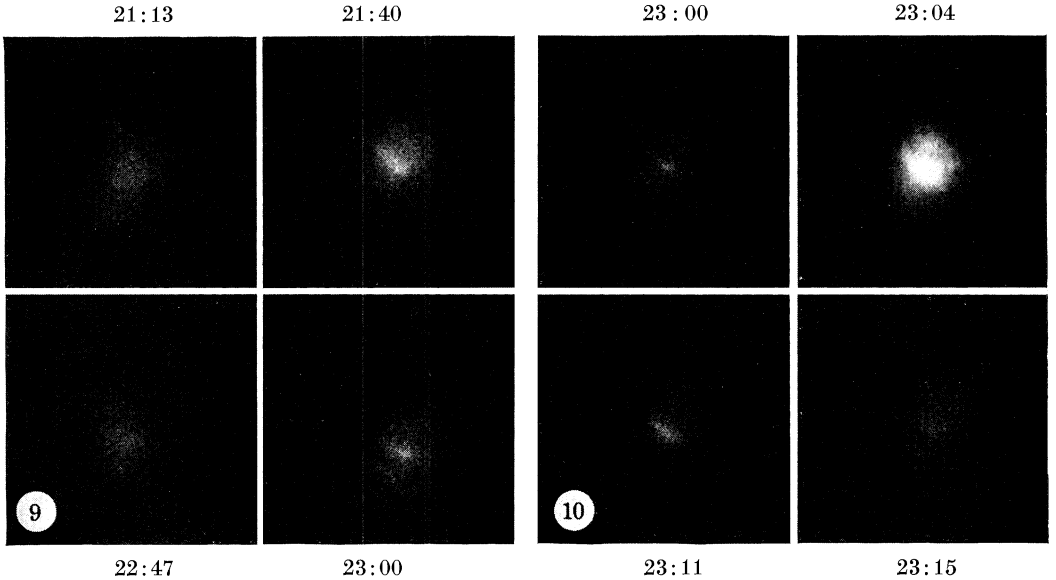

FIGURE 9. A time sequence (G.M.T.) of a simple bipolar region on 1 September 1973, showing short-term variation.

FIGURE 10. Later short-term sequence of the bipolar region of figure 9; note the flaring at 23 h 04 G.M.T.

DESCRIPTION OF PLATE 17

FIGURE 7. A series of images of two active regions, a young and an older one, showing structures of different sizes. (*a*) 4 s exposure, filter 1 (hard) on 5 July 1973 at 13 h 08 U.T., showing the cores, (*b*) 16 s, filter 1 at 13 h 09 U.T., showing compact loop assemblies, (*c*) 4 s, filter 3 (soft) at 13 h 15 U.T., showing interconnections and temperature differences of loops (compare with (*b*)), (*d*) 16 s, filter 3 at 13 h 16 U.T., showing connection to outside regions, (*e*) 64 s, filter 3 at 13 h 17 U.T., showing surrounding structure.

FIGURE 8. A full disk, 256 s, filter 3 view of the 'quiet' Sun on 5 July at 13 h 21 U.T. locating the regions of figure 7 and showing various large-scale loop structures.

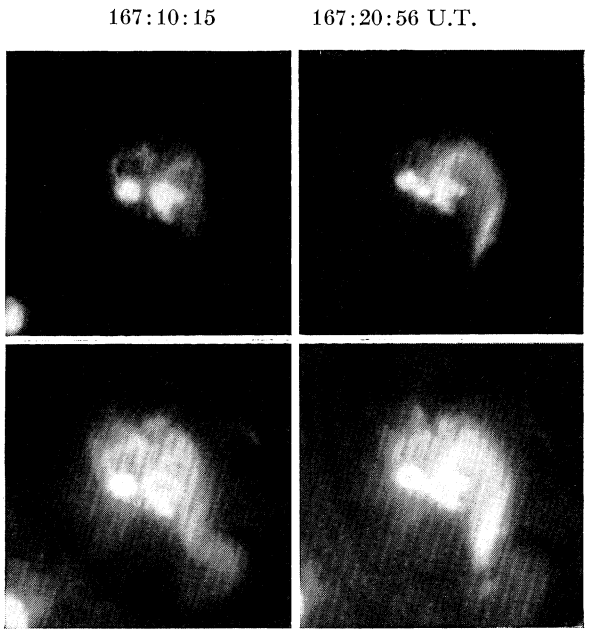

FIGURE 11. Structure of the active region of figure 6 on 16 June 1973 with exposures through hard (upper row) and soft (lower row) filters, indicating structural and temperature variations.

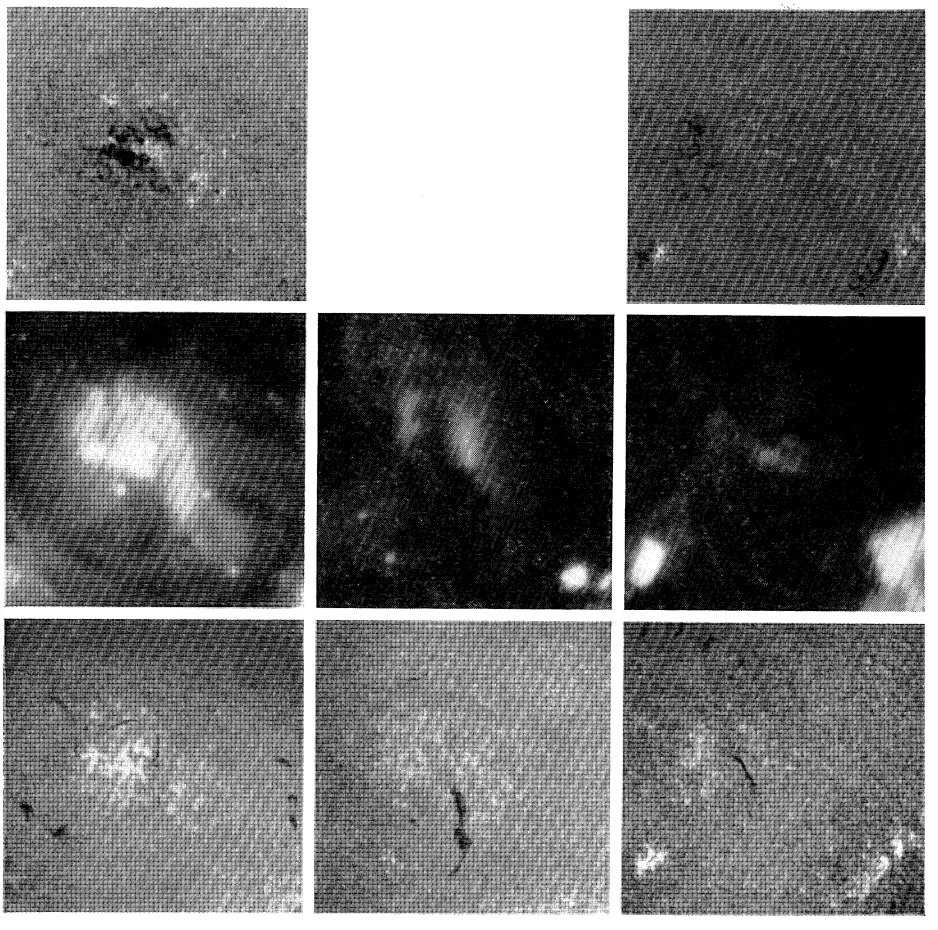

FIGURE 12. The development of the active region of figure 6 over three solar rotations, shown in Kitt Peak magnetogram, X-ray, Hα.

PHILOSOPHICAL TRANSACTIONS OF THE ROYAL SOCIETY A MATHEMATICAL, PHYSICAL & ENGINEERING SCIENCES

The magnetic field associated with the observed features can also be analysed. Small-scale closed configurations occur as bright spots (see Golub *et al.* 1974) which appear in a more or less uniform distribution on the Sun. Magnetic field comparisons show these to be associated with small, bipolar field regions at the photospheric level. Larger-scale plasma loops, ranging from the compact portions of active regions to the large-scale structure covering most of the Sun, appear as connections between fields of opposite polarity.

In addition to these closed magnetic configurations, open structures are also observed in the later stages of development of active regions. The regions overlaying 'filament cavities' appear to fall into this category. Observations of helmet streamers seen by the HAO instrument in white light, over these regions of low coronal material density, appear to indicate there are open configurations surrounding the lower X-ray features that arch around the cavities.

A second type of diverging, open structure is the coronal hole. This feature appears to play an important role as a source of high-velocity solar wind streams, where the plasma can preferentially escape due to the open field configuration (Krieger *et al.* 1974). The coronal hole also appears to display rigid rotation characteristics (Timothy, Krieger & Vaiana 1975). The dark area in the centre and at the pole of figure 3 is an excellent example of this type of feature. The diverging nature of the structures at the boundaries, along with the generally 'unipolar' character of the photospheric field within the region, indicates that an open configuration is present. The weak emission from these holes (faintly observable at the limb) is less than an order of magnitude smaller than from nearby quiet regions and appears to be an indication of the relative absence of hot material. Figure 4, plate 16, illustrates the relation of the photospheric field, shown in a Kitt Peak magnetogram, to the X-ray corona, as well as showing the appearance of the region in Hα and Ca K.

Thus, the magnetic field configuration appears to be strongly associated with the X-ray features observed in the corona. The closed magnetic configuration evidenced by loops appears in all size-scale ranges from the small, bipolar bright points to the largest-scale loops of old active region remnants. This includes the loops associated with the strong, bipolar fields of active regions, from those in the compact portion to those connecting the regions with surrounding areas of opposite field polarity or with other active regions. Open magnetic field configurations also are present in the form of filament cavities and coronal holes. The importance of the magnetic field can be seen in the examples of active region structure and development in the following discussion.

3. Active regions

In this section we concentrate on the general aspects of the structure and evolution of active regions. It turns out that the study of the structure and evolution of active regions is central to an understanding of solar X-ray emission, since most of the emission from the X-ray corona is related either directly or indirectly to solar activity.

First we examine, with increasing complexity, the structure of active regions. Figure 5, plate 16, illustrates the appearance of a simple active region on 1 September 1973. The X-ray image indicates the presence of a central loop seen in projection against the disk. Figure 6, plate 18, shows structures in an active region from 14 June to 17 June 1973 on two size scales (see Vaiana *et al.* 1973*b*). The X-ray images were taken through a hard filter (2–18 Å bandpass). The shorter exposures (top row) highlight the compact structures and show the changes which occur on the time scale of about one day. The dynamics of active regions will be discussed in more detail below.

The longer exposures (bottom row) display a more complex structure for the region over the same period. Larger, complex loop assemblies can clearly be discerned. Also shown are the corresponding magnetic fields (in the Kitt Peak magnetograms of the middle row).

In figure 7, plate 17, we present a series of images indicating the different size scales present in active regions. Two regions of 5 July 1973 are displayed, a young one, that is brighter in its core and more compact, and an older one, that is larger and somewhat more diffuse. The shortest exposure, 7*a*, in the hard filter (2–18 Å) is 4 s and distinguishes the compact core of the young region as a few bright, well-defined loops of a size of approximately $10'' \times 50''$. A 16 s exposure in the same filter, 7*b*, reveals larger assemblies of loops in the compact regions and emphasizes the contrast and brightness differences between the two regions. Figure 7*c* is a 4 s exposure in the softest filter (2–32, 44–55 Å). Additional, larger-scale features are clearly evident, including connections between the two regions. One difference is that of temperature in the emitting feature, with the softer filter showing cooler regions not seen with the harder filter. The size of the large interconnecting loop is visually estimated to be about $20'' \times 300''$. Comparison of data from the two filters allows us to determine a typical temperature of about 3×10^6 K for active regions (ranging from about 2×10^6 K for older, larger loops to about 4×10^6 K for cores).

In the 16 s exposure (figure 7*d* of the sequence) much more detail is brought out, and we now see connections to regions outside the active region. The 64 s, soft filter image, 7*e*, displays further loop structure of sizes up to about $30'' \times 500''$. In addition structure can be observed in the bright spots distributed throughout the photograph. A final, full disk image (figure 8, plate 17) with a 256 s exposure in the soft filter is included to provide the location of these regions and to display fainter details of the large-scale structure on the Sun.

We now turn our attention to the dynamics of active region development and consider changes that occur on various time scales. First, we examine those which occur over a few minutes in simple active regions.

Figures 9 and 10, plate 18, show a sequence of photographs of the very simple bipolar region shown in figure 5 (a few arc seconds across) at time intervals ranging from 3.5 to 7 min. Clearly this region is highly variable on the time scale illustrated here. In the middle of the sequence (23 h 04 G.M.T.) the region flares and then subsides. The similarity of the initial and final photographs illustrates the point that the structure of the region was essentially unchanged by the flare. R. D. Petrasso, who has studied this event in detail (Petrasso *et al.* 1975), has reached the very important conclusion, with regard to the localization of the flare trigger, that it takes place in a very localized region consistent with a location coincident with the pre-existing small loop. This again emphasizes the loop as a fundamental structure of the low corona. Flares are a characteristic of the short-term variability of active regions. For a statistical study establishing

---

Description of plate 20

Figure 13. Soft (upper row) and hard (lower row) views of the active region of figure 12 over the same three rotations.

Figure 15. A series of images during the emergence of a small active region with 64 s exposures in filter 1. (*a*) 00 h 32 U.T. on 2 September 1973, (*b*) 03 h 54 U.T. on 2 September, (*c*) 13 h 14 U.T. on 2 September, and (*d*) 13 h 14 U.T. on 4 September.

Figure 16. A 16 s, filter 1 sequence of the same active regions as figure 15. (*a*) 00 h 31 U.T. on 2 September 1973, (*b*) 03 h 52 U.T. on 2 September, (*c*) 13 h 13 U.T. on 2 September, and (*d*) 13 h 13 U.T. on 4 September.

Figure 17. The active regions of figure 15 in a 16 s, filter 3 series. (*a*) 00 h 20 U.T. on 2 September 1973, (*b*) 13 h 32 U.T. on 2 September, and (*c*) 13 h 03 U.T. on 4 September.

PHILOSOPHICAL TRANSACTIONS OF THE ROYAL SOCIETY A MATHEMATICAL, PHYSICAL & ENGINEERING SCIENCES

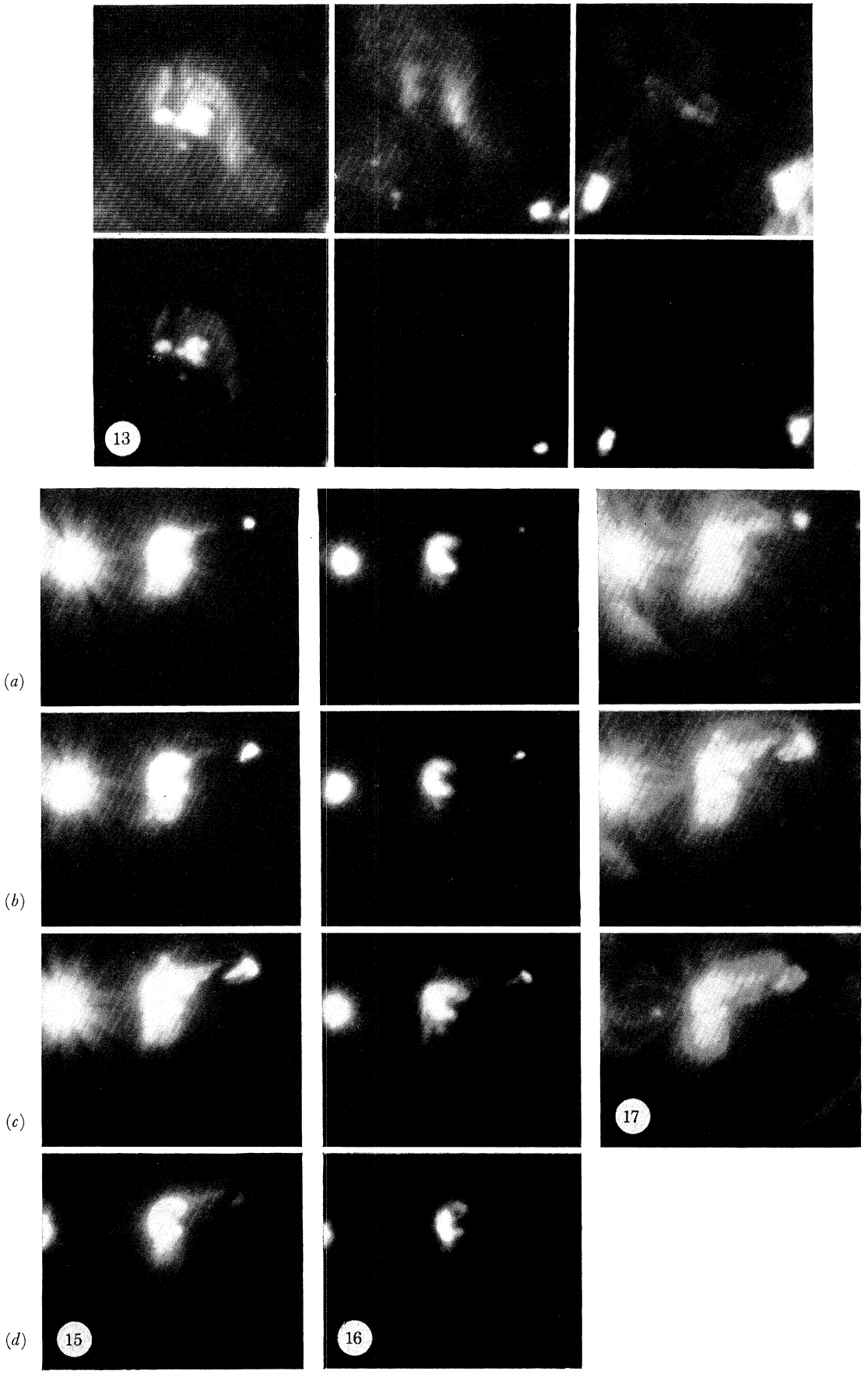

FIGURES 13 AND 15–17. For description see opposite.

(*Facing p.* 370)

PHILOSOPHICAL TRANSACTIONS OF THE ROYAL SOCIETY A MATHEMATICAL, PHYSICAL & ENGINEERING SCIENCES

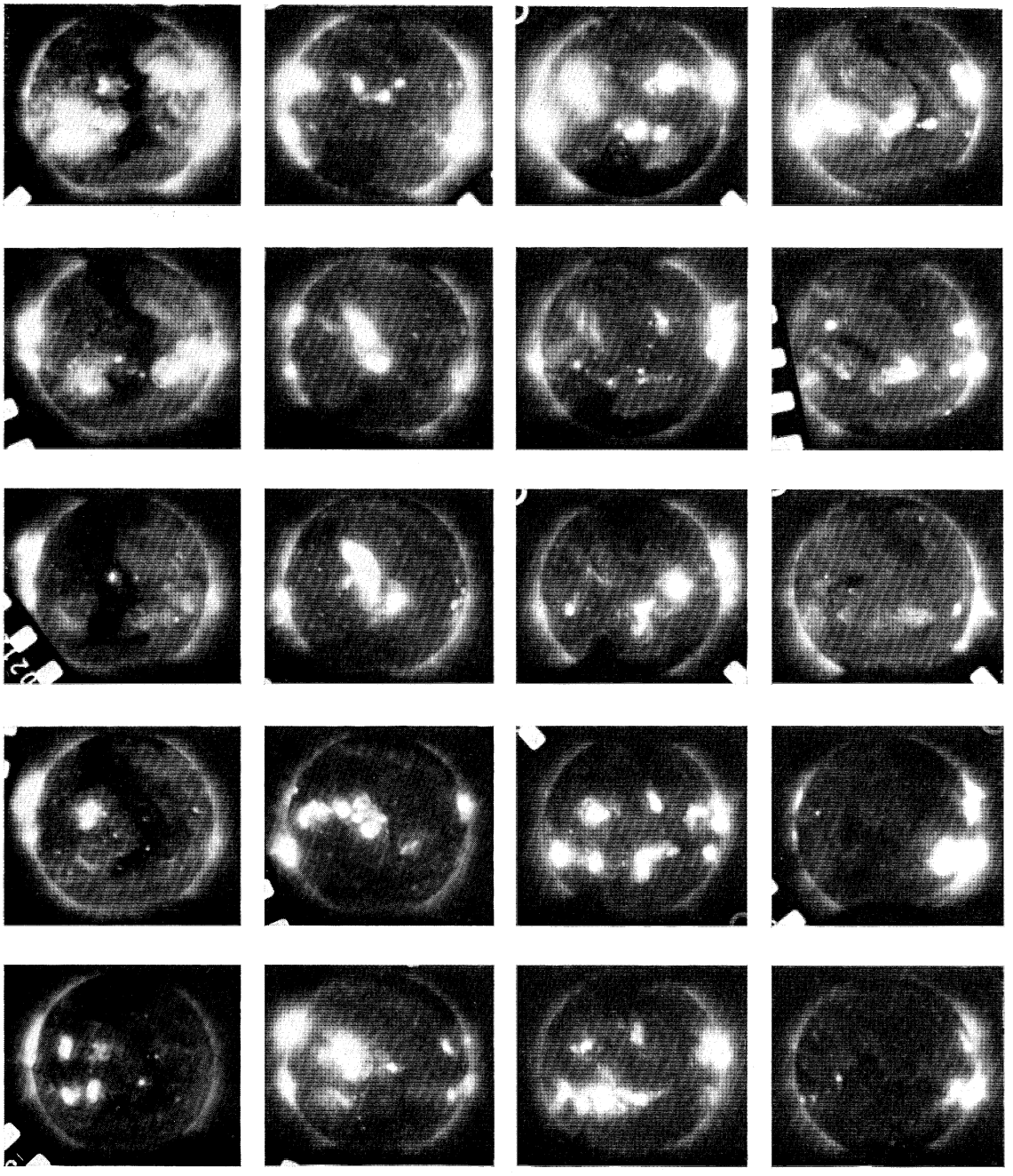

FIGURE 14. (*a*) Sequence of X-ray images for the first five solar rotations during the Skylab missions. (Each row represents one rotation.) (*b*) The corresponding dates for (*a*) and schematic diagrams of the images locating some features according to a letter code described in the text.

PHILOSOPHICAL TRANSACTIONS OF THE ROYAL SOCIETY A MATHEMATICAL, PHYSICAL & ENGINEERING SCIENCES

the localized presence of X-ray 'kernels' in a class of flares observed by Skylab, see Kahler, Krieger & Vaiana (1975).

Next we consider somewhat longer-term variations. Let us again examine figure 6, which shows the X-ray structure of an active region, its relation to the photospheric magnetic field, and its time development over three days, with a time resolution of approximately 10 h. Examination

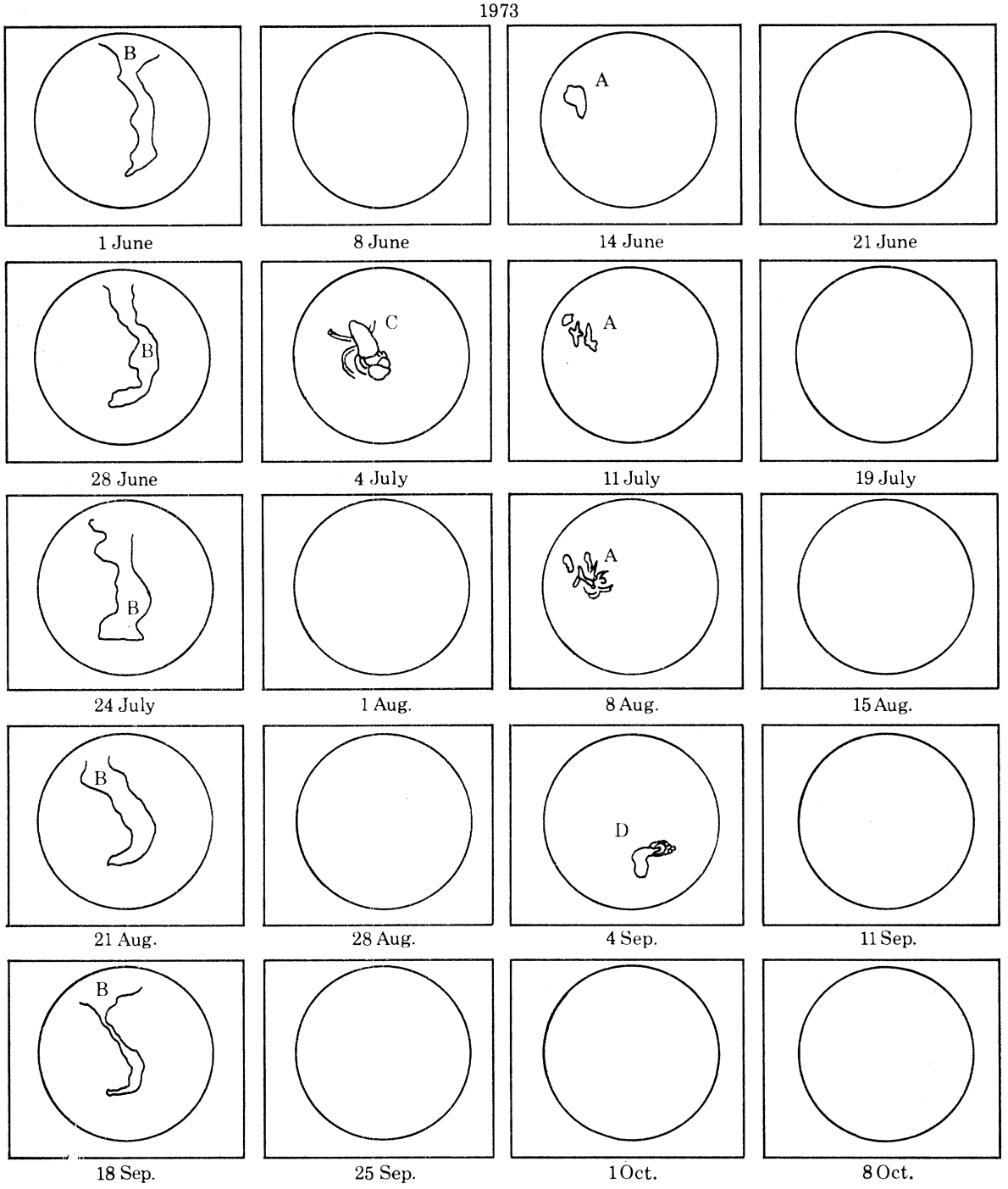

FIGURE 14(*b*). For description see opposite.

PHILOSOPHICAL TRANSACTIONS OF THE ROYAL SOCIETY A MATHEMATICAL, PHYSICAL & ENGINEERING SCIENCES

of the data with higher time resolution shows changes similar to the ones observed in figures 9 and 10. The compact portion of the active region is related to strong magnetic field gradients approximately perpendicular to the neutral line. Larger loops coming out from these compact regions show changes over a time scale of days, but it is difficult to disentangle the changes in the magnetic structure from the changes associated with heating of the plasma. Clear evidence for a temperature variation can be seen in images of the same active region, 10 h apart, with a soft and a hard filter (figure 11, plate 19). If we look at the sequence with the hard filter (upper row), the topology of the magnetic field appears to have changed drastically. The soft-filter photograph indicates, however, that at least part of the magnetic field configuration might have existed at the time of the first exposure, with the matter being at a lower temperature. In any case figures 6 and 11 make the point that large changes occur in coronal active regions over a period of a day.

Over a longer period of time active regions may undergo significant changes. An example of such a long-term change is given in figure 12, plate 19, which shows the long-term variation of an active region over three solar rotations. The corresponding variations in Hα photographs and magnetograms all show the same general evolution: a spreading out, weakening with age, and finally a merging into surrounding larger-scale features.

Figure 13, plate 20, is a sequence of photographs of the same three rotations with two different filters. It shows that there is a definite decline in the temperature of the active region as it spreads out. By the third solar rotation the active region has become undetectable through the hard filter, which is sensitive only to temperatures greater than about 2×10^6 K.

This active region can be seen in the third column of figure 14*a*, which presents X-ray images of five of the solar rotations observed during the mission. For a single column, each row is separated from the next by about one solar rotation, and each column corresponds to about a 90° rotation from the previous column. Similar presentations have been prepared for the rest of the mission. Figure 14*b* gives the corresponding dates for 14*a* and schematic diagrams of some of the regions, with various features mentioned in the text located on the disk by letters. In addition to the active region above, denoted by the letter A, there are the coronal hole B of figures 3 and 4 (over several rotations), the active region C of figure 7, and the emerging region D discussed below and shown in figures 15, 16 and 17, plate 20. In general, we can follow the evolution of active regions down the columns, noting a spreading out and weakening with age, and finally a merging into the surrounding larger-scale features. This long-term evolution is complicated by the interaction with new emerging regions. The coronal holes represent the final breakdown of the thermal plasma confinement at an altitude lower in the corona than for the surrounding areas.

We now turn our attention to the study of the emergence of active regions. Sheely *et al.* (1974) studied one such emergence for 2 September 1973. The A.S. & E. experiment also observed this region in several sequences of images. These covered the entire period of 2 September through 3 September with 2 h or better time resolution between sequences (often only minutes separating the sequences), except during 7 h (05 h 43–12 h 48 U.T.), when no data were recorded. A few of the images are shown in figures 15, 16 and 17. Figure 15 is a sequence of 64 s exposures in filter 1 over a period of $2\frac{1}{2}$ days. Figure 16 is a corresponding sequence of 16 s exposures in the same filter, showing more inner structure, while figure 17 represents a series of 16 s exposures in filter 3, showing additional surrounding structures. In 15*a*, 16*a*, and 17*a*, the small region has already partly emerged (*ca.* 0 h U.T. on 2 September 1973). Three and one-half hours later (15*b*, 16*b* – no corresponding filter 3 image), the small region has emerged somewhat more and now shows an

almost flare-like compact core, but no major changes have occurred in the surrounding structure despite the flaring of a nearby active region. A little less than 10 h later (15 *c*, 16 *c*, 17 *b*) the region has shown considerable change, and the large, nearby region is more clearly connected to the smaller one by a large loop structure. Also, there are now two loops extending from the small region, while its core has subsided. Finally, 2 days later the small region and the connecting structures have become much more diffuse.

Study of different sequences of images, thus, leaves the impression that there is, over different time scales, a variety of changes occurring in active regions from their emergence to their dispersion. There are the short-term changes presented, of which flare activity is an extreme manifestation, and in which the topology may or may not change. And there are also the long-term changes in which the large-scale structure of an active region undergoes significant change and in which interaction with large coronal structures occurs.

4. Discussion

Finally, let us summarize some of the results which emerge from the quantitative analyses of the data:

(1) Regions of high temperature are typically associated with regions of high density (see table 1) – an important point which suggests that the pressure gradients present require non-force-free currents for equilibrium.

(2) Excluding flares and, perhaps, some cores of active regions, the temperatures of the different structures vary only by a factor of 2, from 1.5×10^6 K to 3×10^6 K, while characteristic lengths vary by a factor of 10, and densities by a factor of 20 or more.

(3) Bright points behave like miniature active regions, with similar dispersal parameters, but with somewhat lower densities. Their presence at very high latitudes, however, implies a mechanism for their generation different from that in active regions.

(4) The cooling times (10^3–10^4 s – see table 1) are in every case less than the characteristic lifetimes of the structures (with the possible exception of flares), so a continuous input of energy is required. Any breakdown in the energy balance will be reflected by variations on a time scale on the order of t_{rad}, or shorter if conductive cooling is dominant.

(5) High enough densities (10^9–10^{10} cm^{-3}) are reached so that in the loop configuration radiation losses are often significant – several times 0.1 J cm^{-2} s^{-1}. The ratio between radiative losses and conductive losses for a loop with a scale distance between footpoints R_9 (in units of 10^9 cm), a density N_9 (in units of 10^9 cm^{-3}), and a temperature T_6 (in units of 10^6 K) is given by

$$L_{\mathrm{r}}/L_{\mathrm{c}} \simeq 4.5 \times 10^{-3} N_9^2 T_6^{-\frac{5}{2}} R_9 \pi \beta \gamma^{-2},$$

where β is a form factor ($\frac{1}{2}\pi$ for circular loops) and γ is the constriction factor for the cross-sectional diameter in the foot points compared to the diameter in the corona. From this expression it can be seen that the predominance of radiation over conduction will depend critically on the constriction factor γ.

(6) The densities in flares are much larger than in the coronal structures, and flares comprise relatively large volumes, implying that chromospheric material is being heated.

(7) If one includes radiation between 50 and 100 Å, most of the solar X-ray luminosity is contributed by the large-scale structures and has a value of a few times 10^{20} J s^{-1}.

These points, along with the general structure and evolution of active regions and the corona

PHILOSOPHICAL TRANSACTIONS OF THE ROYAL SOCIETY A MATHEMATICAL, PHYSICAL & ENGINEERING SCIENCES

as a whole as presented earlier, provide us with an overview of some of the processes occurring in the X-ray corona.

The development of the S-054 X-ray telescope and the subsequent analysis of the data obtained from Skylab required the efforts of a large number of people. Among them are R. Chase, J. Davis, L. Golub, M. Gerassimenko, S. Kahler, A. Krieger, J. Nolte, R. Petrasso, R. Simon, J. Silk and D. Webb of A.S. & E.; A. Timothy at N.A.S.A. Headquarters; and C. Maxson and M. Zombeck at the Center for Astrophysics.

References (Vaiana)

Golub, L., Krieger, A. S., Silk, J. K., Timothy, A. F. & Vaiana, G. S. 1974 Solar X-ray bright points. *Astrophys. J.* **189**, L93–L97.

Kahler, S. W., Krieger, A. S. & Vaiana, G. S. 1975 Morphological analysis of X-ray flare structures from the rise through the decay phase. (Submitted to *Astrophys. J. Lett.*)

Krieger, A. S., Timothy, A. F., Vaiana, G. S., Lazarus, A. J. & Sullivan, J. D. 1974 X-ray observations of coronal holes and their relation to high velocity solar wind streams. (To be published in *Proceedings of the Third Solar Wind Conference, Asilomar Conference Grounds, Pacific Grove, Calif.*, 25–29 *March*; *Reviews of Geophysics and Planetary Physics*.)

Petrasso, R. D., Kahler, S. W., Krieger, A. S., Silk, J. K. & Vaiana, G. S. 1975 The location of the site of energy release in a solar X-ray subflare. (Submitted to *Astrophys. J. Lett.*)

Sheely, N. R., Jr., Bohlin, J. D., Bruecker, G. E., Purcell, J. D., Scherrer, V. & Tousey, R. 1974 XUV Observations of coronal magnetic fields. Naval Research Laboratory preprint.

Timothy, A. F., Krieger, A. S. & Vaiana, G. S. 1975 The structure and evolution of coronal holes. (To be published in *Solar Phys.*)

Vaiana, G. S., Krieger, A. S. & Timothy, A. F. 1973*a* Identification and analysis of structures in the corona from X-ray photography. *Solar Phys.* **32**, 81–116.

Vaiana, G. S., Davis, J. M., Giacconi, R., Krieger, A. S., Silk, J. K., Timothy, A. F. & Zombeck, M. 1973*b* X-ray observations of characteristic structures and time variations from the solar corona: preliminary results from Skylab. *Astrophys. J.* **185**, L47–51.

Vaiana, G. S., Krieger, A. S., Timothy, A. F. & Zombeck, M. 1974*a* ATM observations, X-ray results. Presented at *IAU Colloq. No.* 27, *Harvard College Obs.*, 9–11 *September*.

Vaiana, G. S., Krieger, A. S., Petrasso, R., Silk, J. K. & Timothy, A. F. 1974*b* The X-ray Spectrographic Telescope. *Instrumentation in Astronomy–II, Proc. SPIE*, 4–6 *March*, *Tucson*, *Ariz.*, **44**, 185–205.

PHILOSOPHICAL TRANSACTIONS OF THE ROYAL SOCIETY A MATHEMATICAL, PHYSICAL & ENGINEERING SCIENCES

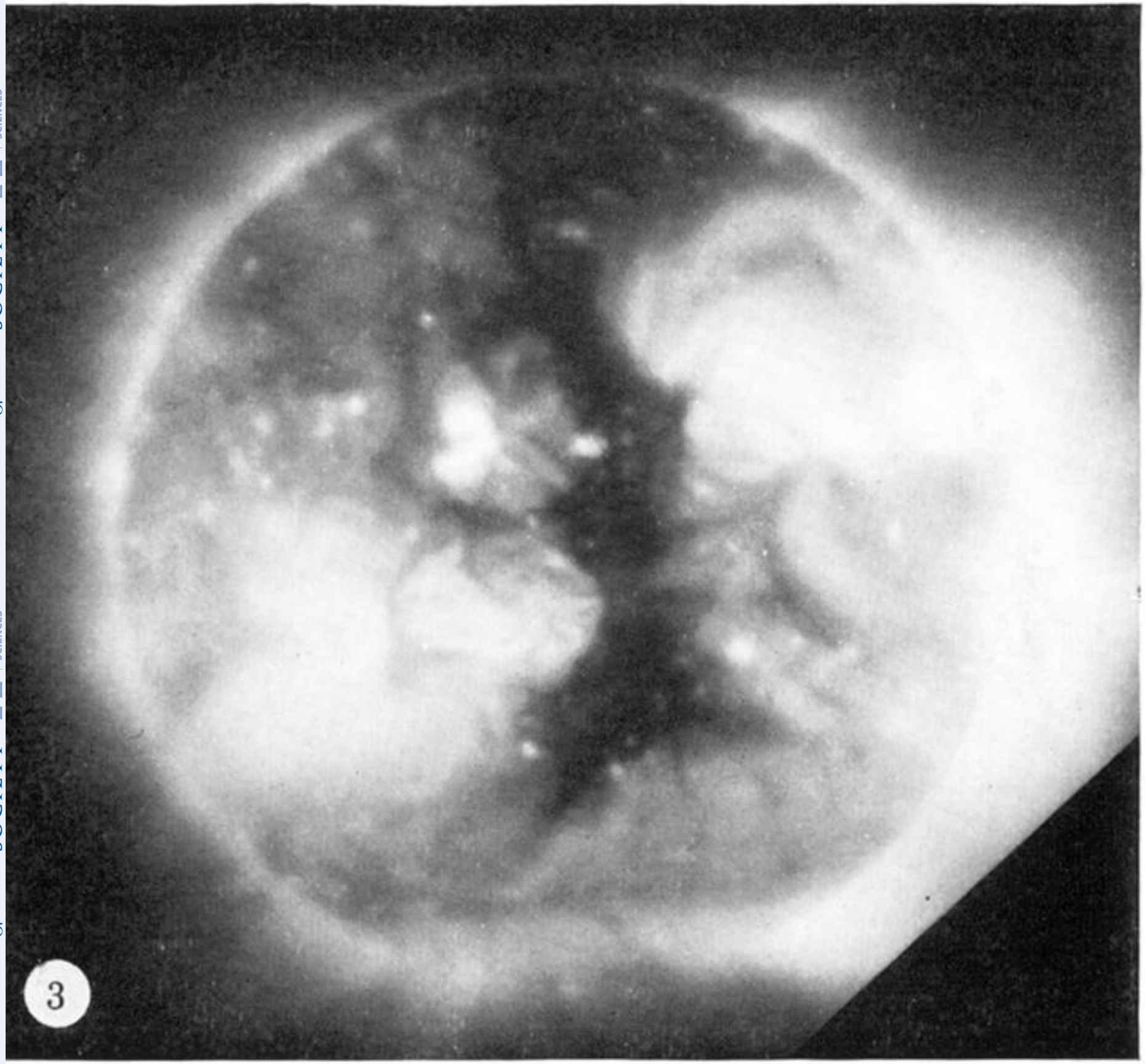

FIGURE 3. A full disk view of the X-ray corona on 1 June 1973.

PHILOSOPHICAL TRANSACTIONS OF THE ROYAL SOCIETY A MATHEMATICAL, PHYSICAL & ENGINEERING SCIENCES

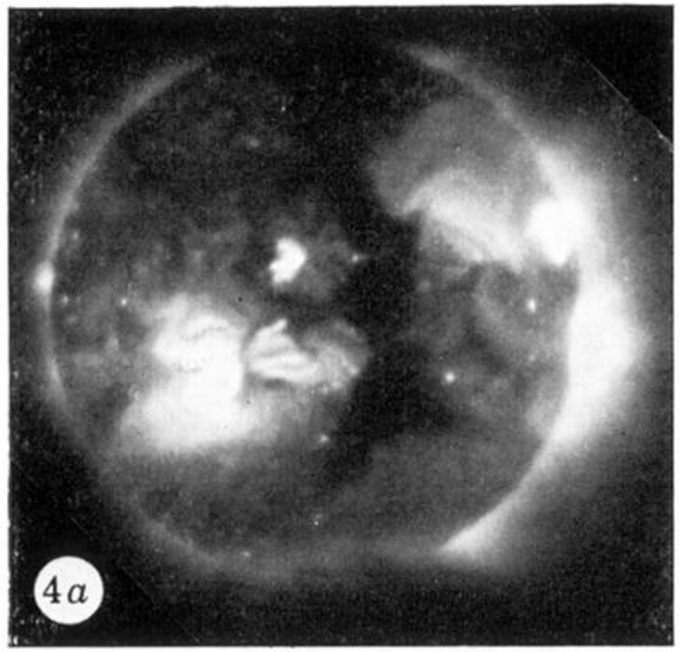

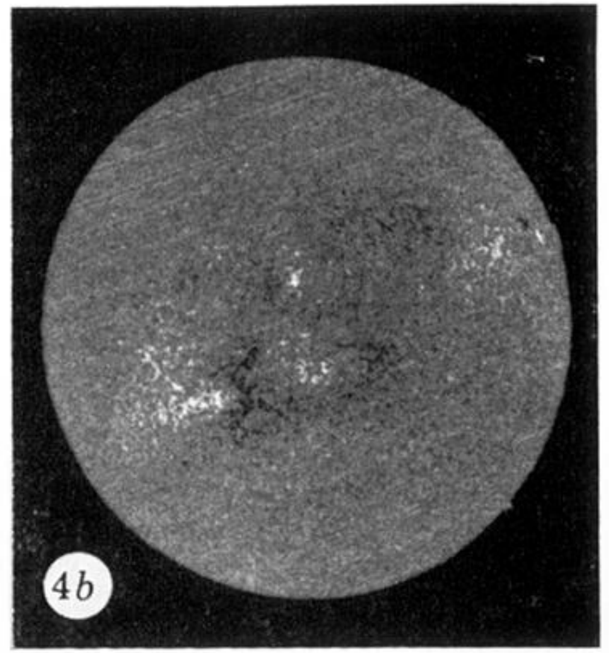

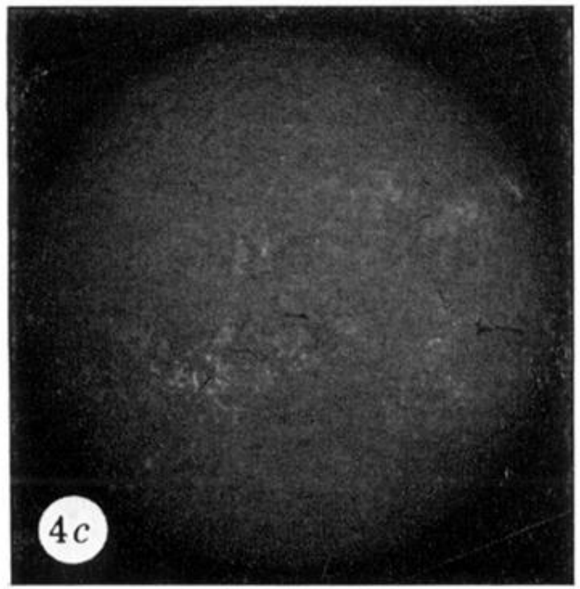

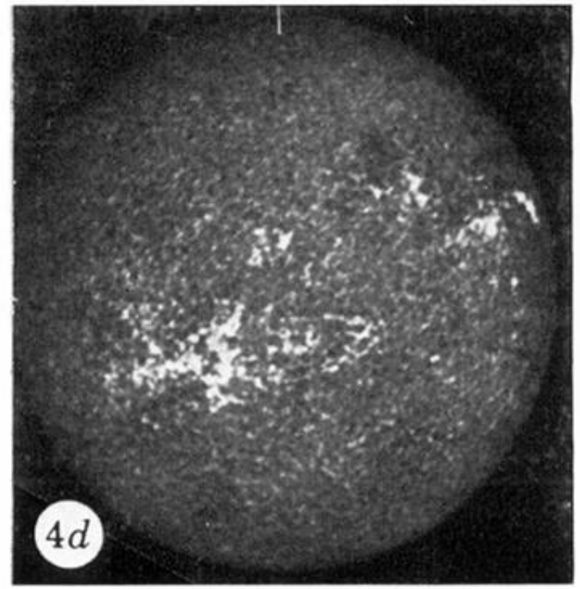

FIGURE 4. Comparison of (*a*) the X-ray corona showing the 1 June 1973 coronal hole with (*b*) the corresponding Kitt Peak magnetogram (courtesy of J. Harvey & W. Livingston), (*c*) an Hα image, and (*d*) a Ca K image for the same date.

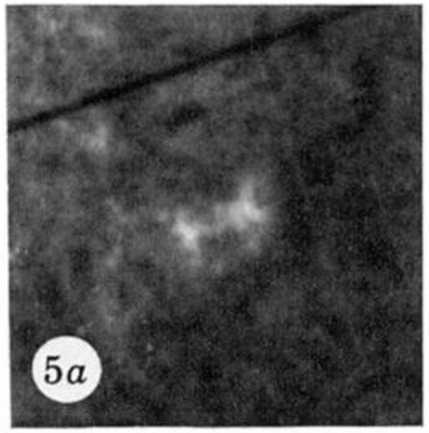

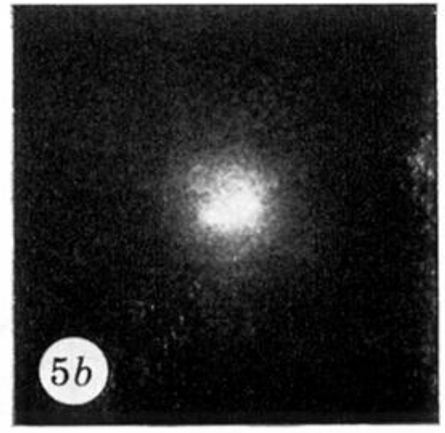

FIGURE 5. (*a*) Hα and (*b*) X-ray images of a very simple active region (22:07:00 U.T. and 21:40:18 U.T. of 1 September 1973). Note the indication of a loop structure in the X-ray core.

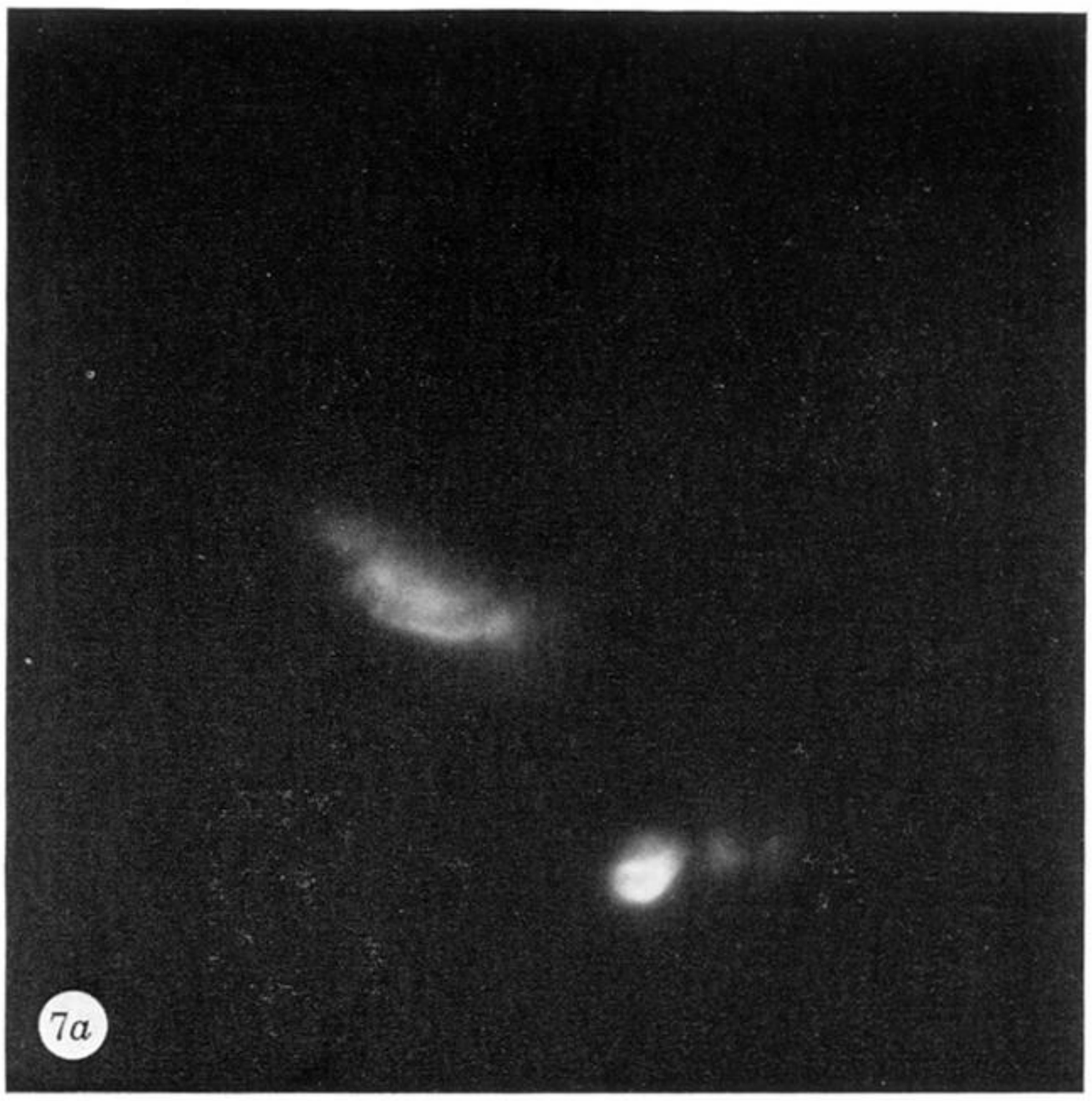

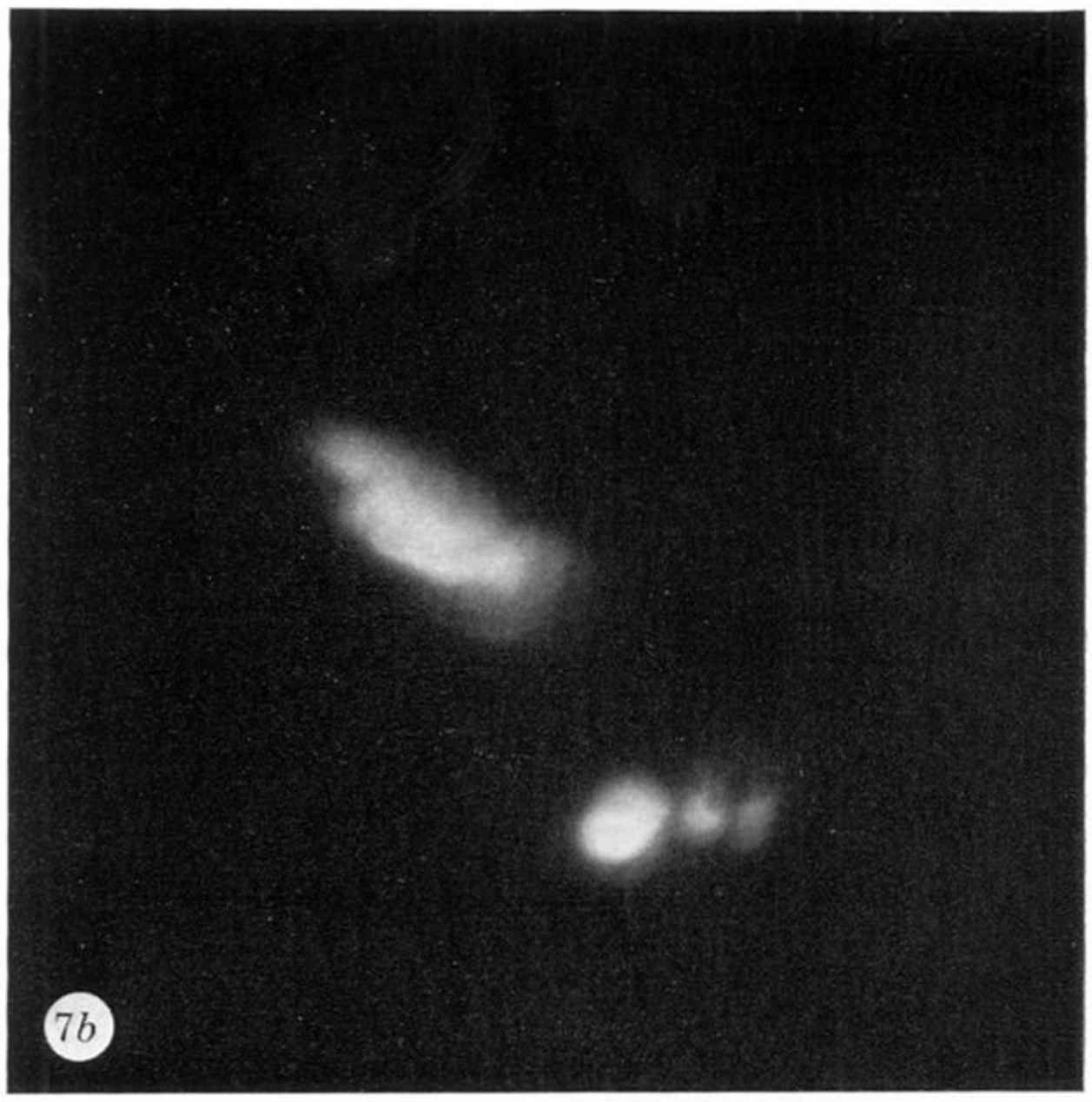

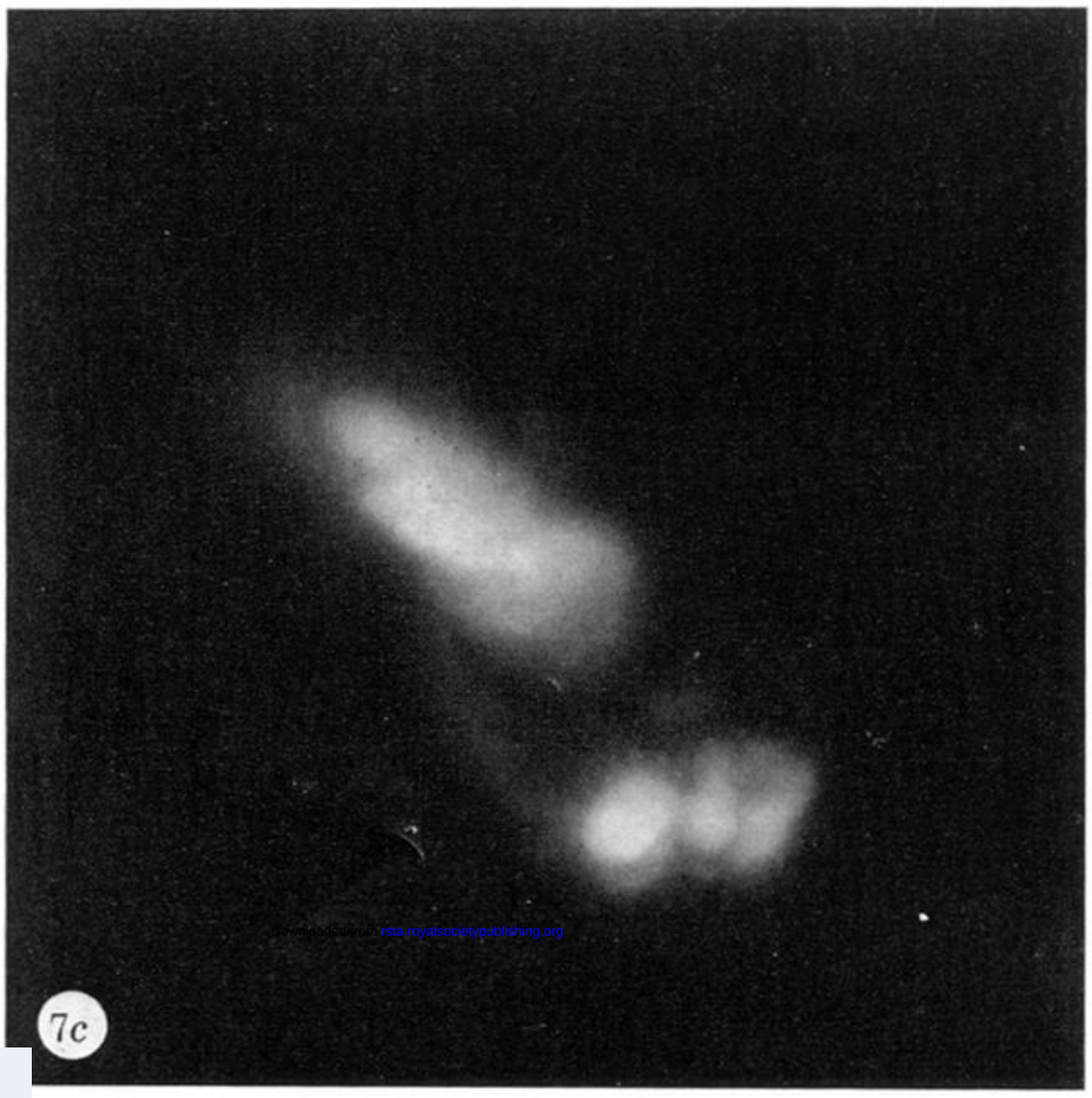

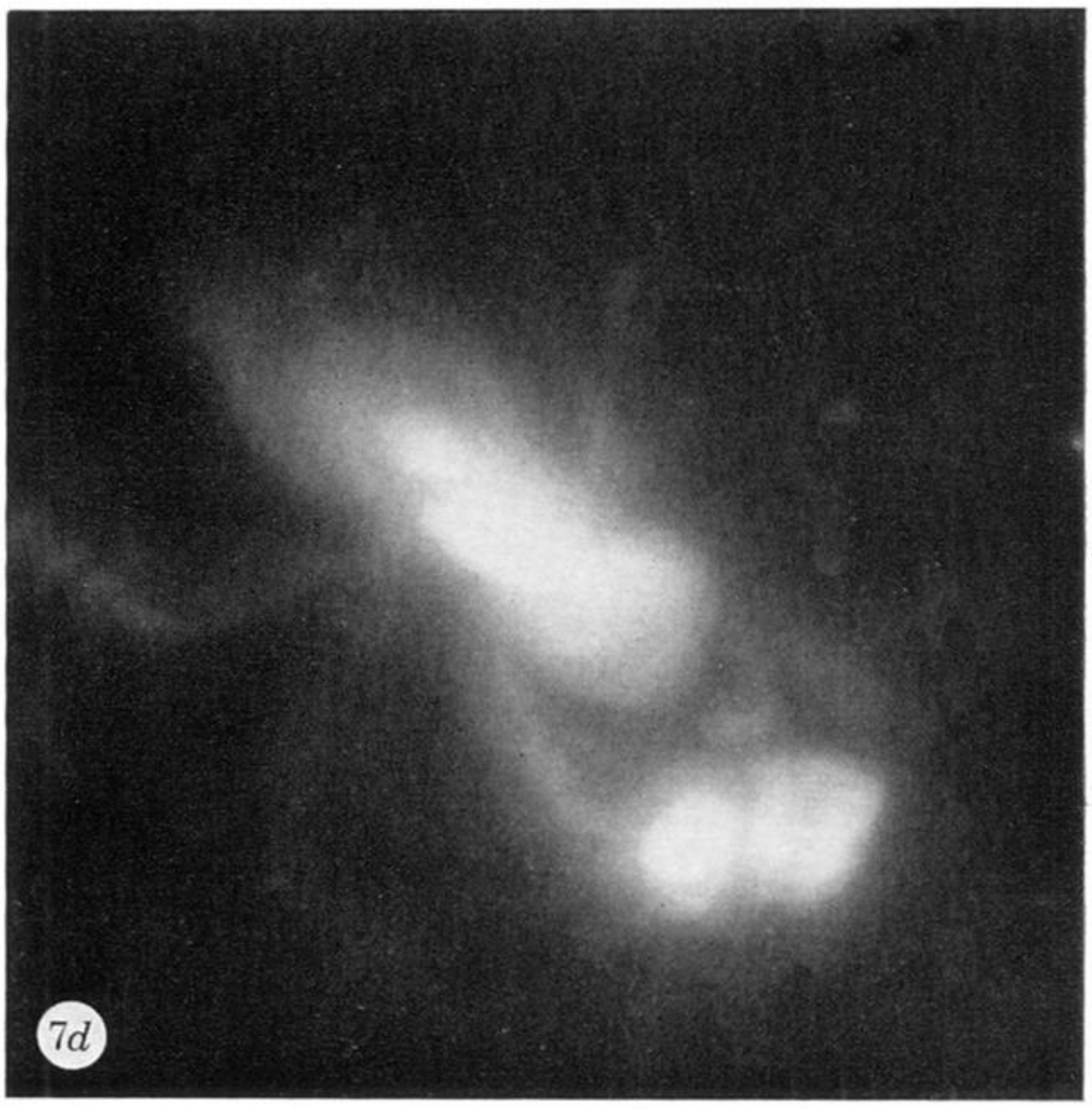

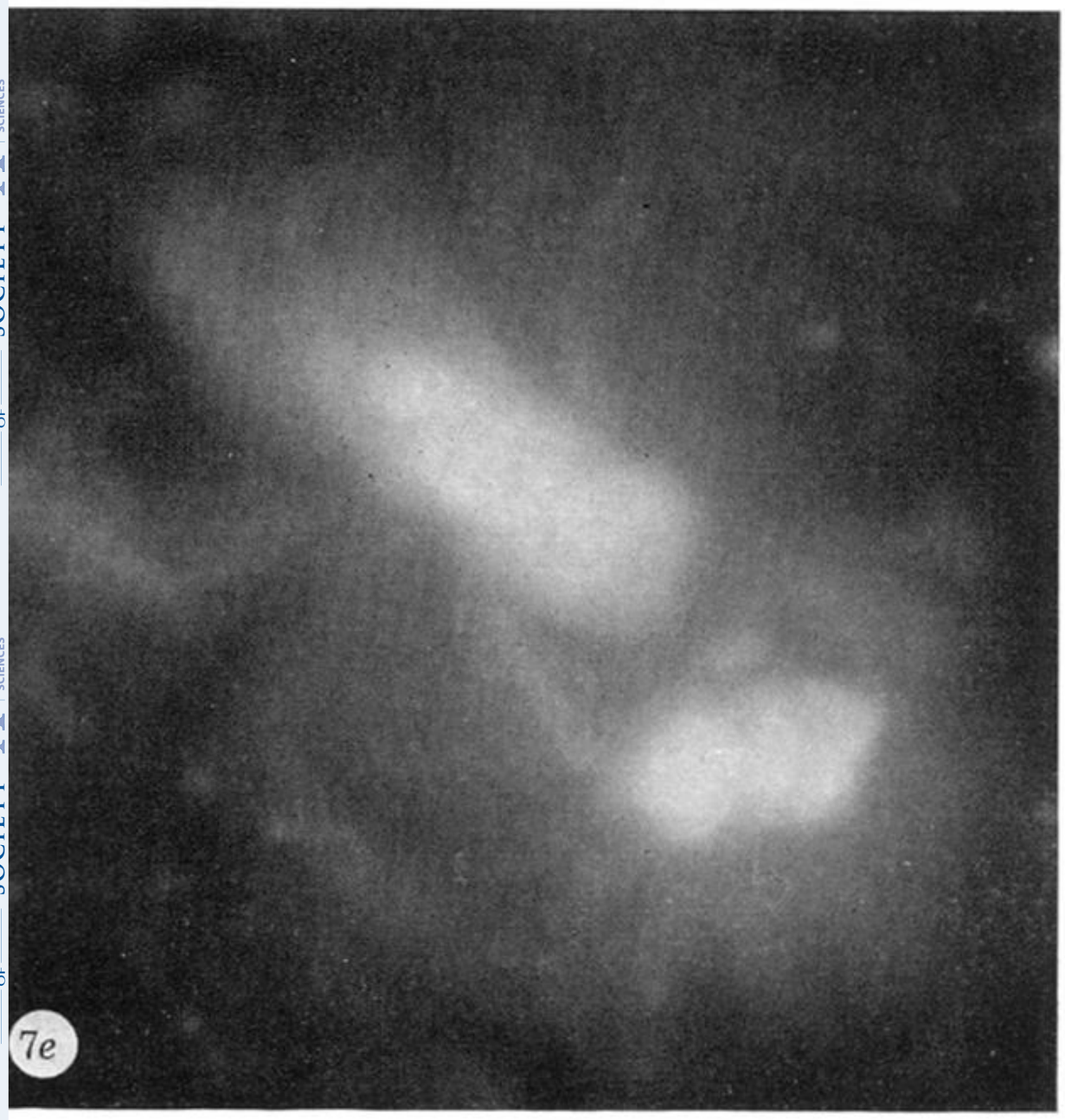

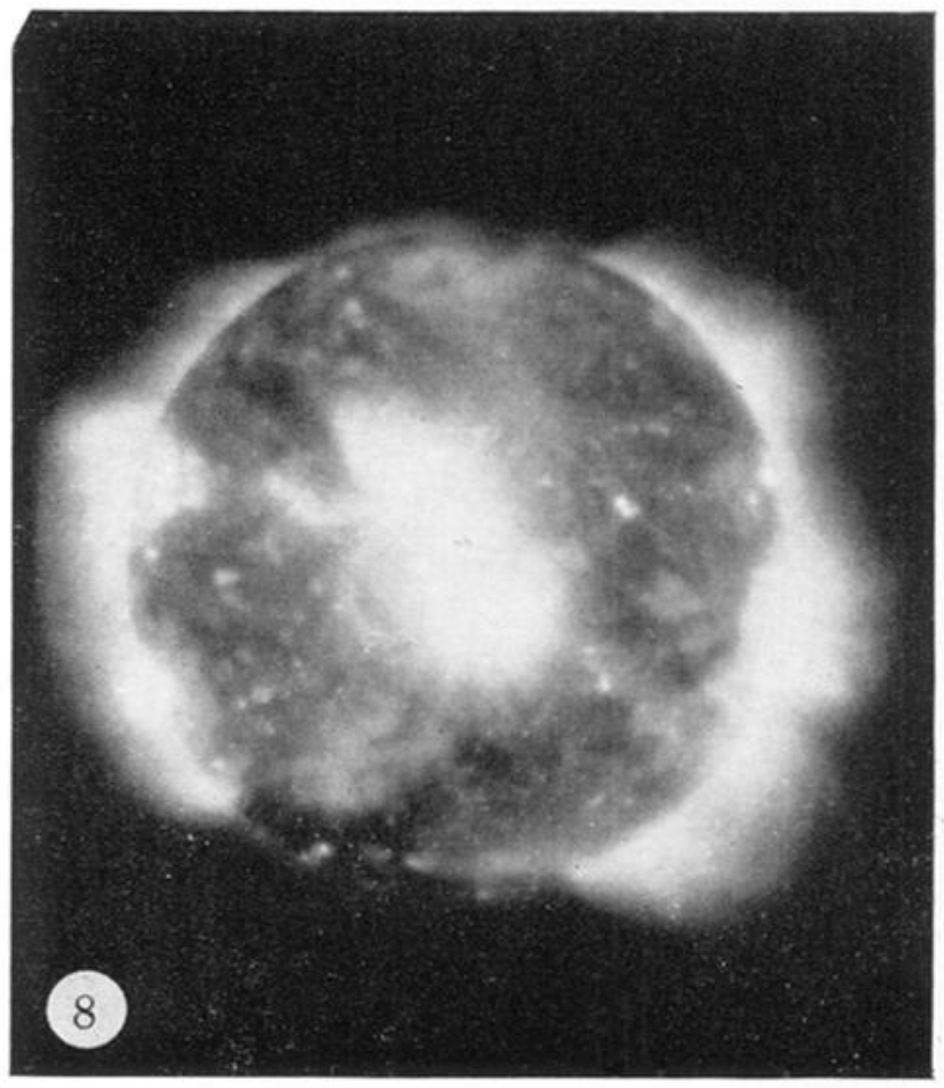

PHILOSOPHICAL TRANSACTIONS OF THE ROYAL SOCIETY A MATHEMATICAL, PHYSICAL & ENGINEERING SCIENCES

FIGURES 7 AND 8. For description see opposite.

top and bottom:	165:13:16	166:21:57	167:21:04	168:21:52
middle:	165:14:23	166:15:07	167:19:17	168:17:34

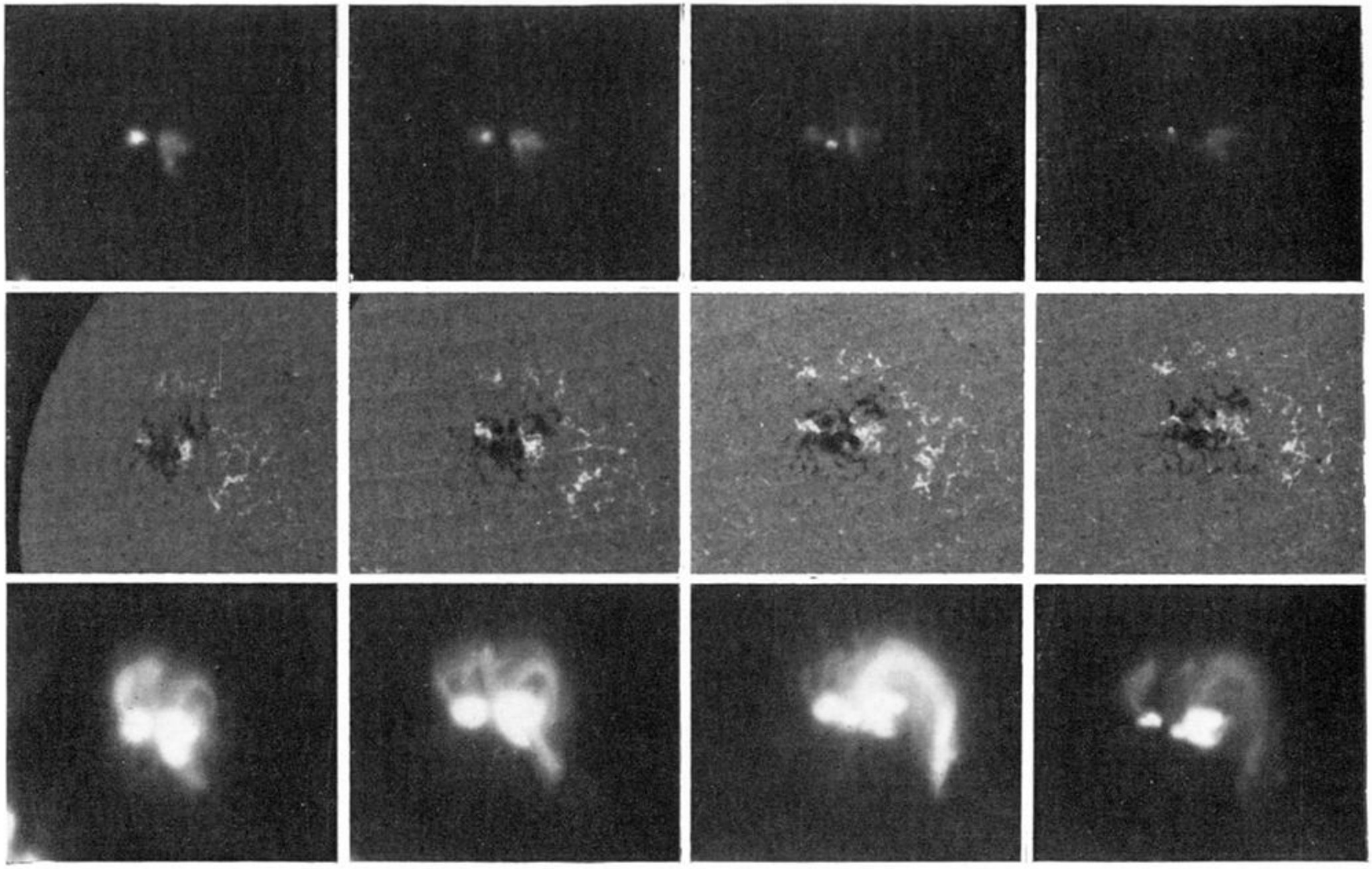

FIGURE 6. A three-day development of an active region from 14 June to 17 June 1973. Both the X-ray images (hard filter, two exposures, top and bottom rows) and the Kitt Peak magnetograms (middle row) are shown. The field is approximately 4×10^5 km by 5×10^5 km for each image.

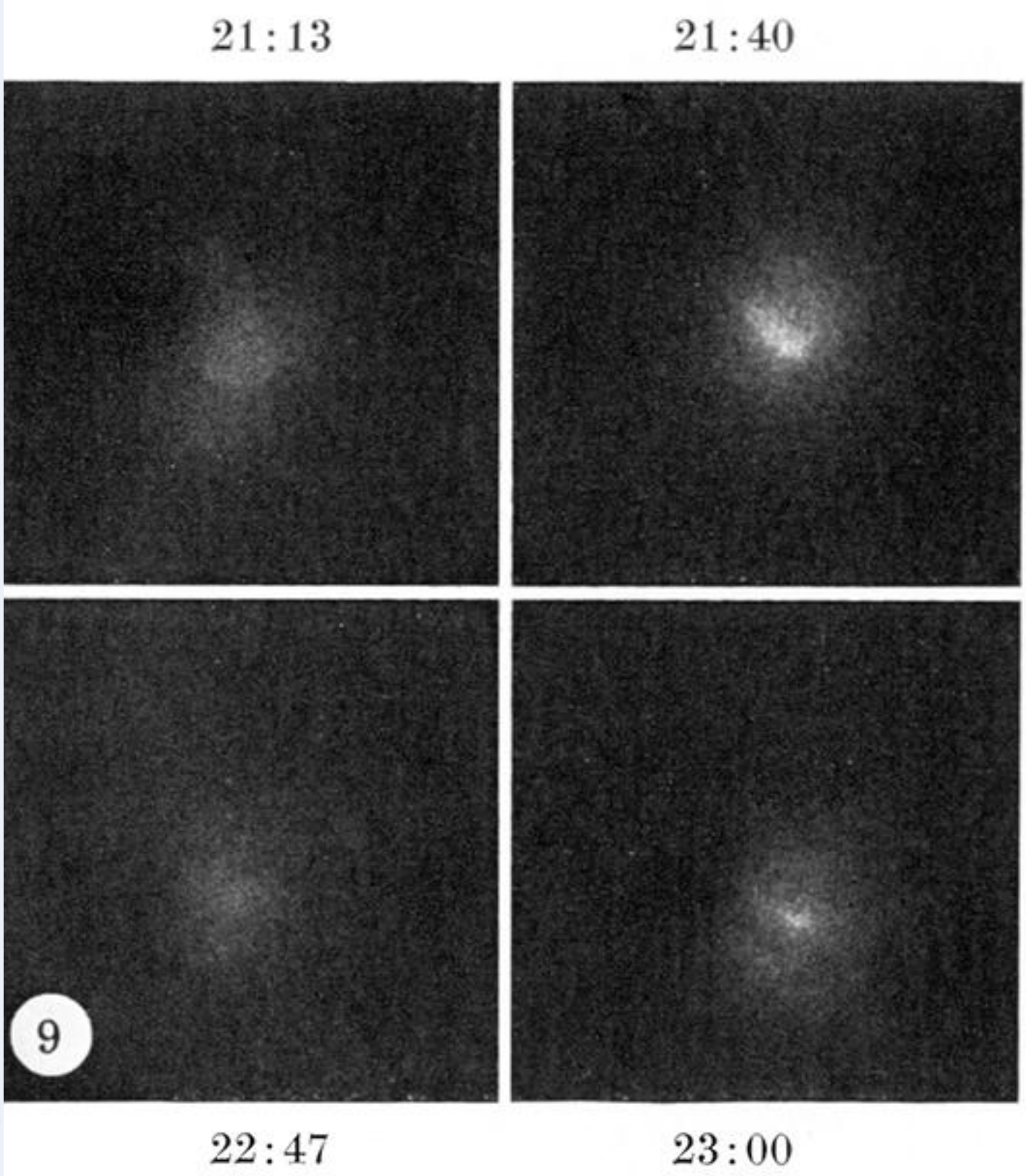

PHILOSOPHICAL TRANSACTIONS OF THE ROYAL SOCIETY A MATHEMATICAL, PHYSICAL & ENGINEERING SCIENCES

FIGURE 9. A time sequence (G.M.T.) of a simple bipolar region on 1 September 1973, showing short-term variation.

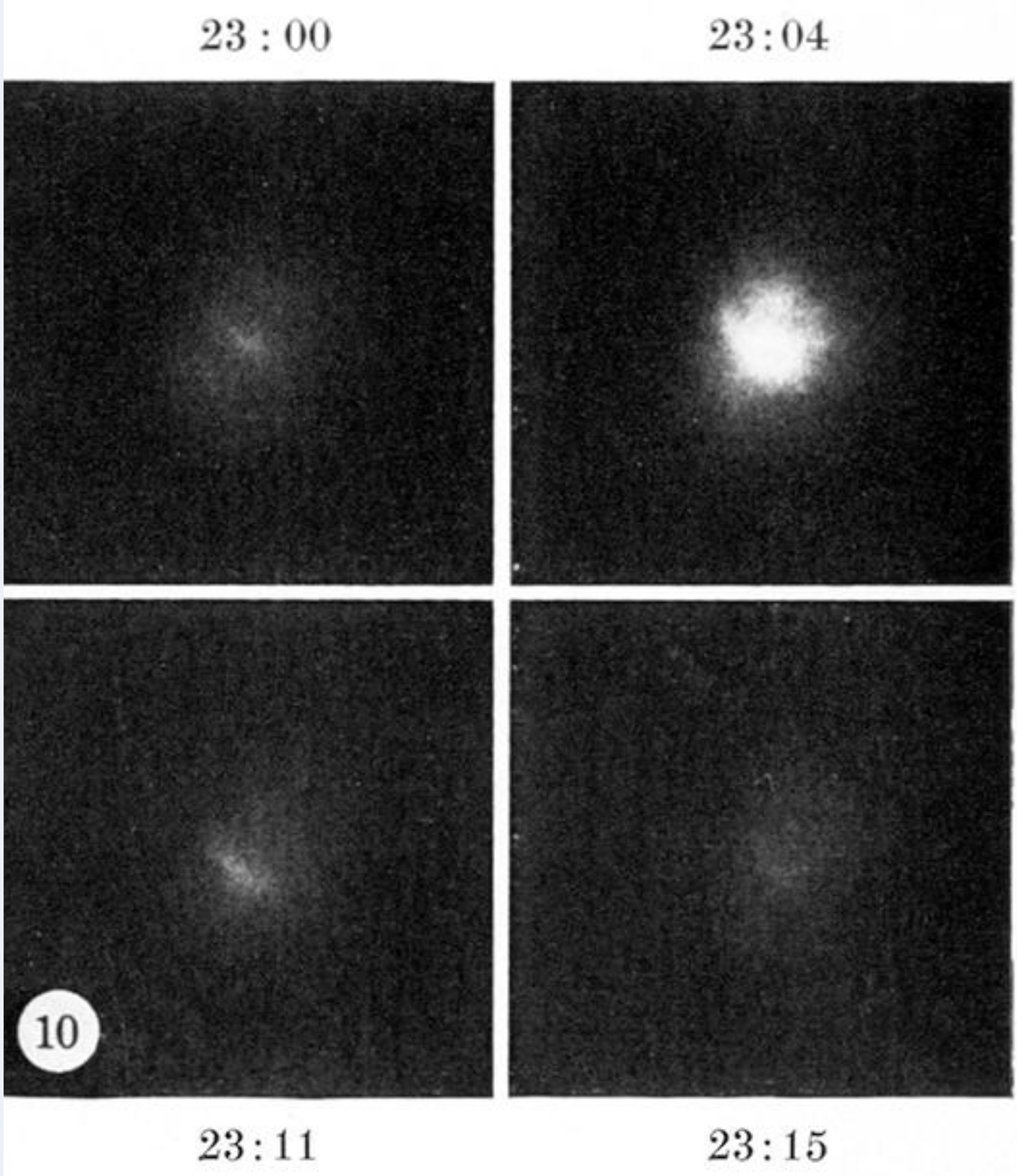

PHILOSOPHICAL TRANSACTIONS OF THE ROYAL SOCIETY A MATHEMATICAL, PHYSICAL & ENGINEERING SCIENCES

FIGURE 10. Later short-term sequence of the bipolar region of figure 9; note the flaring at 23 h 04 G.M.T.

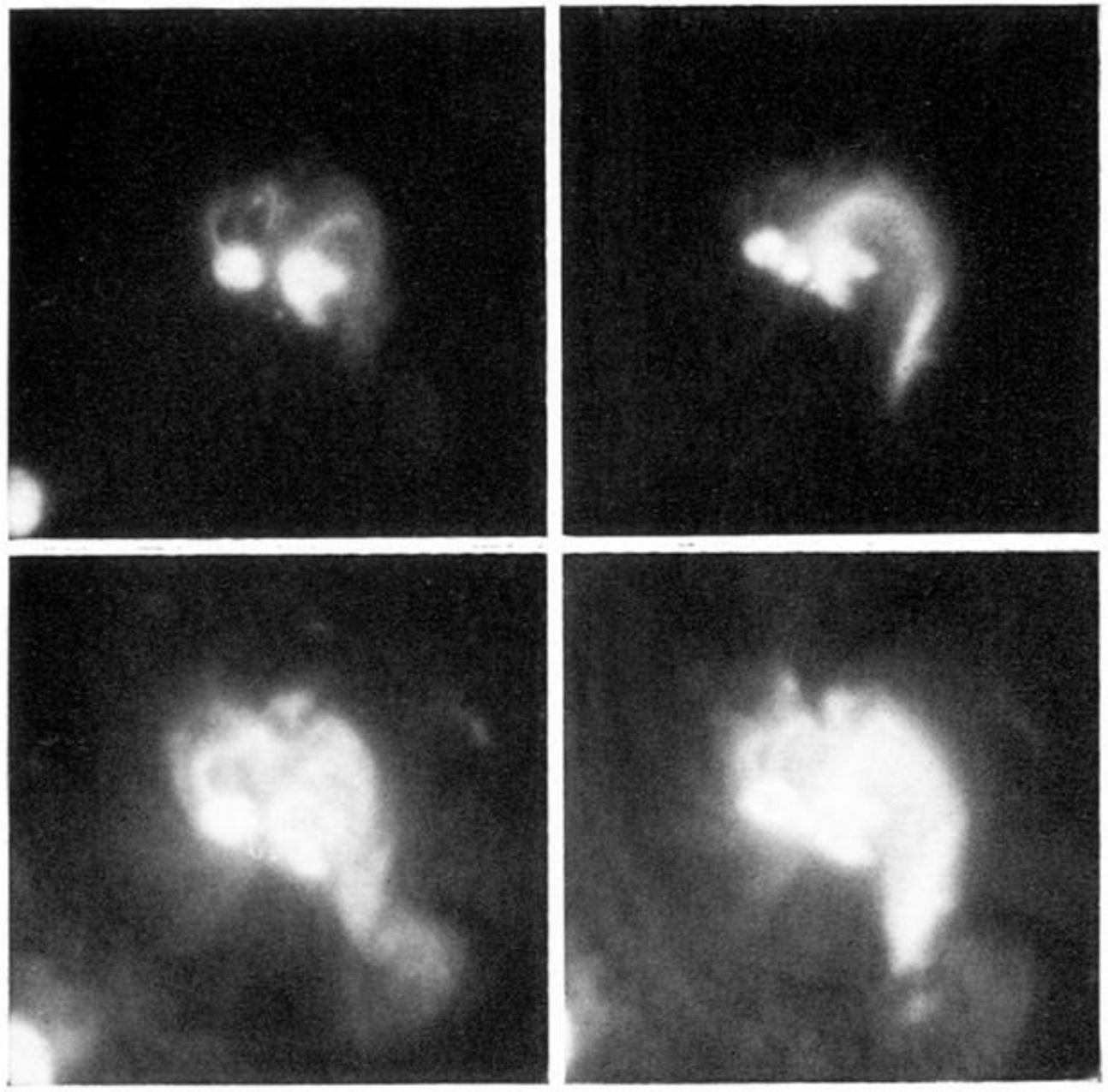

IGURE 11. Structure of the active region of figure 6 on 16 June 1973 with exposures through hard (upper row) and soft (lower row) filters, indicating structural and temperature variations.

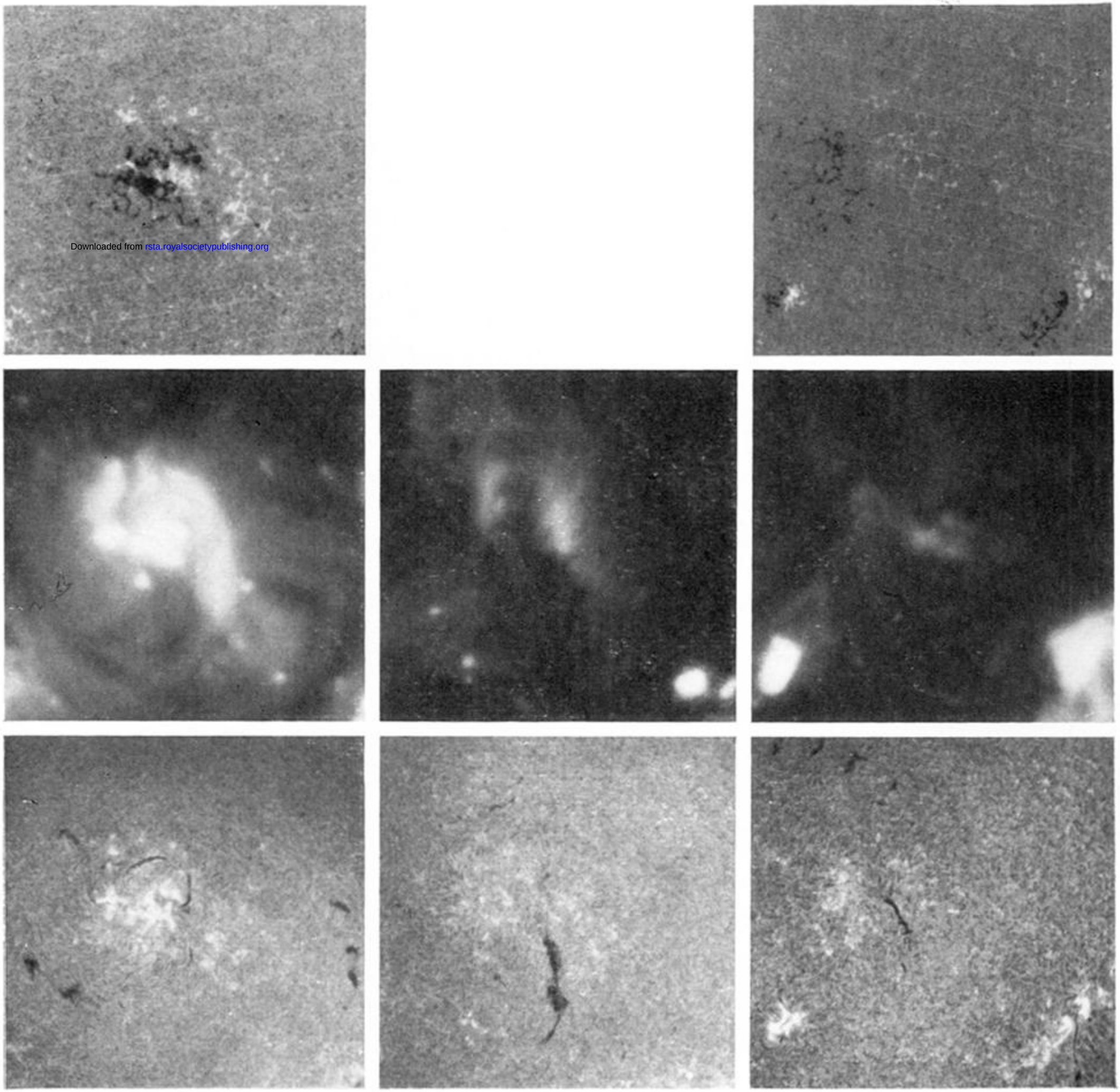

FIGURE 12. The development of the active region of figure 6 over three solar rotations, shown in Kitt Peak magnetogram, X-ray, Hα.

PHILOSOPHICAL TRANSACTIONS OF THE ROYAL SOCIETY A MATHEMATICAL, PHYSICAL & ENGINEERING SCIENCES

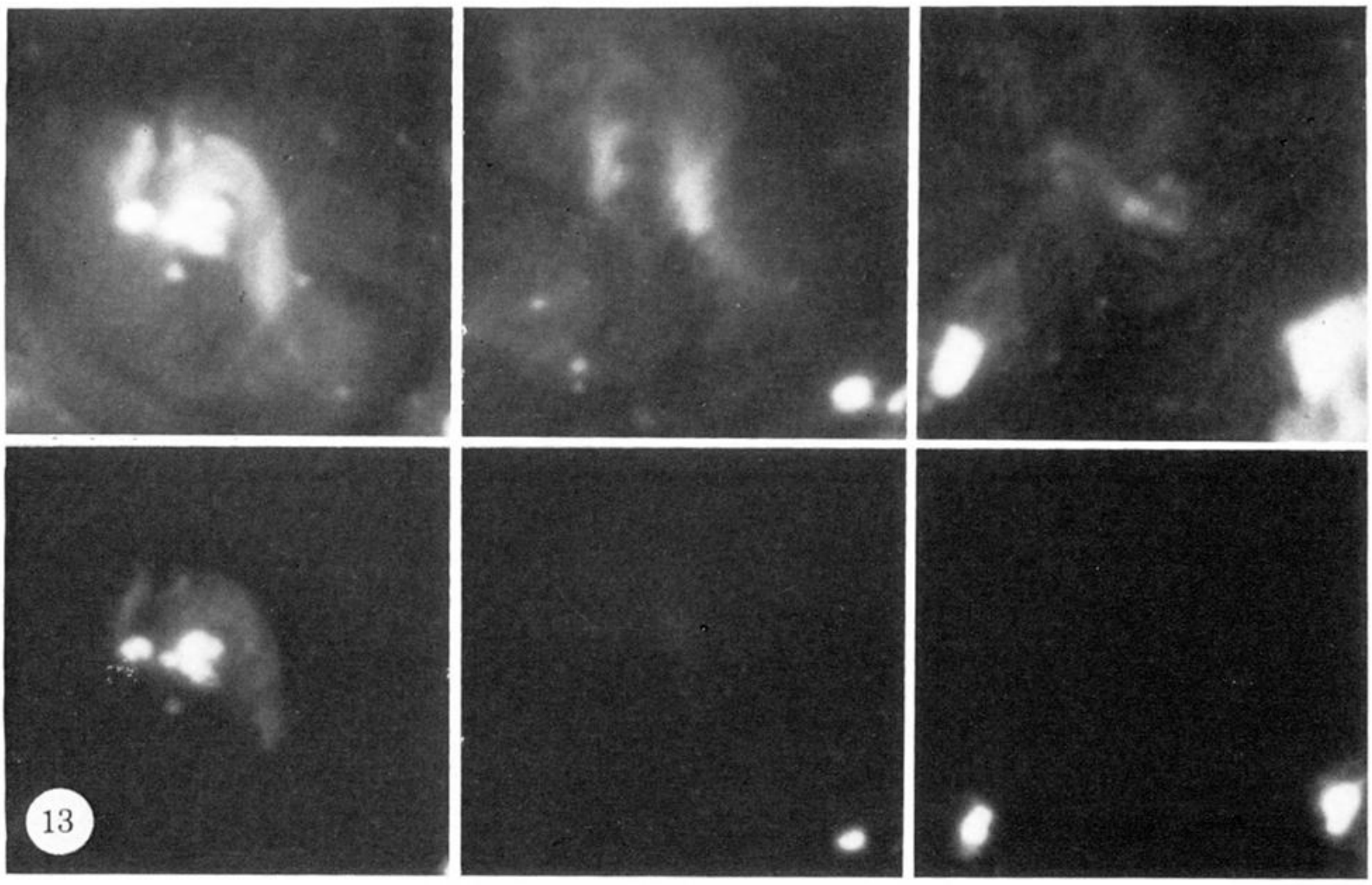

(*a*)

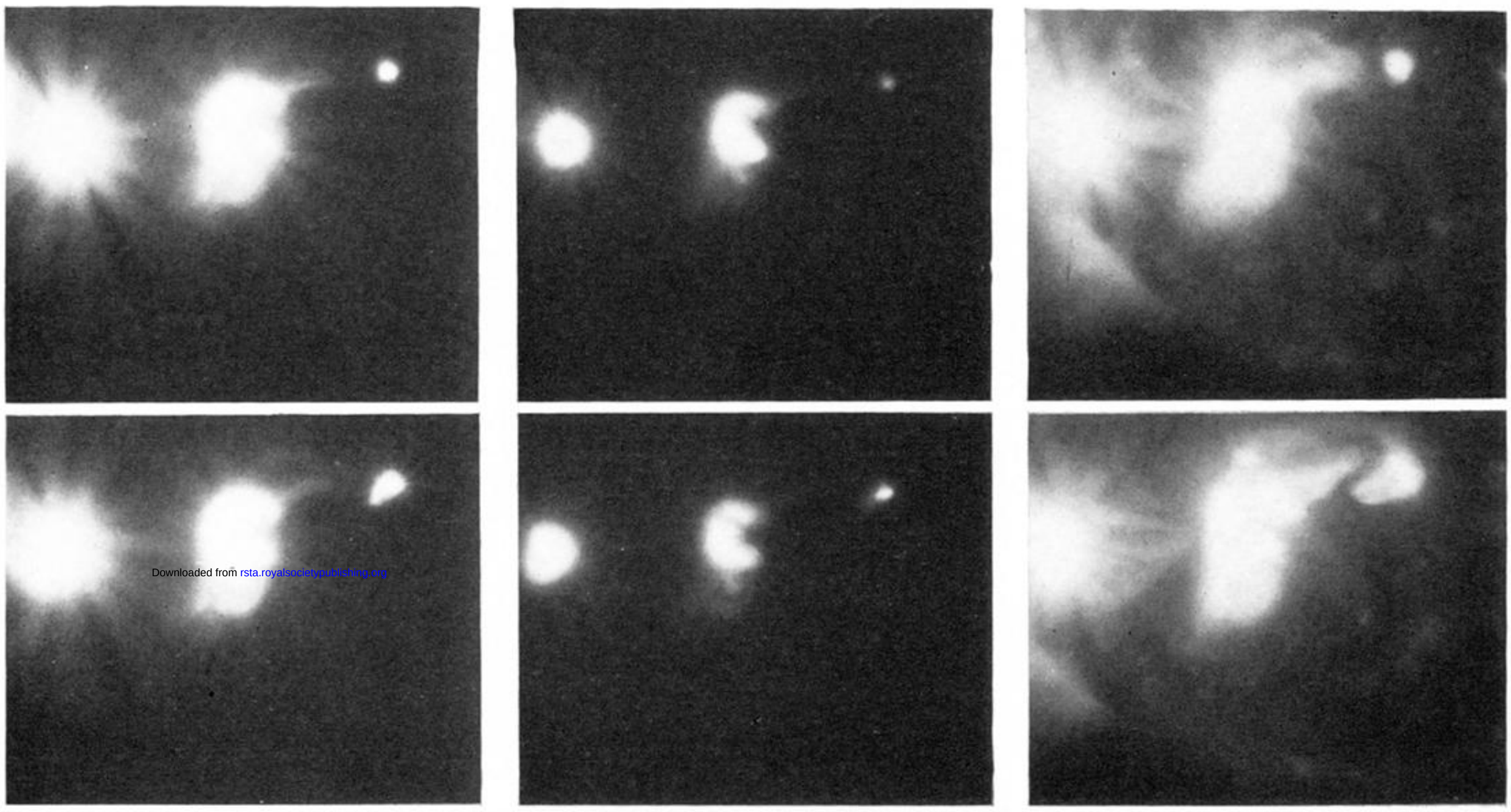

(*b*)

(*c*)

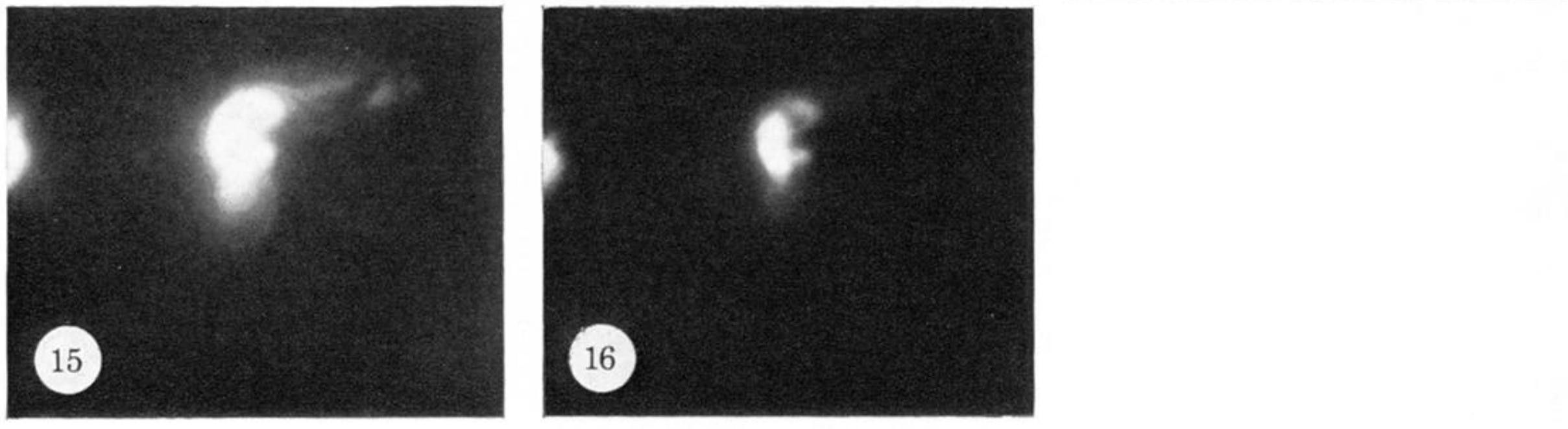

(*d*)

FIGURES 13 AND 15–17. For description see opposite.

FIGURE 14. (*a*) Sequence of X-ray images for the first five solar rotations during the Skylab missions. (Each row represents one rotation.) (*b*) The corresponding dates for (*a*) and schematic diagrams of the images locating some features according to a letter code described in the text.

PHILOSOPHICAL TRANSACTIONS OF THE ROYAL SOCIETY A MATHEMATICAL, PHYSICAL & ENGINEERING SCIENCES